A proposed integrated approach for the preclinical evaluation of phage therapy in Pseudomonas infections

Peer-reviewed author version

Danis-Wlodarczyk, Katarzyna; Vandenheuvel, Dieter; Bin Jang, Ho; Briers, Yves; Olszak, Tomasz; Arabski, Michal; Wasik, Slawomir; Drabik, Marcin; Higgins, Gerard; Tyrrell, Jean; Harvey, Brian J.; NOBEN, Jean-Paul; Lavigne, Rob & Drulis-Kawa, Zuzanna (2016) A proposed integrated approach for the preclinical evaluation of phage therapy in Pseudomonas infections. In: SCIENTIFIC REPORTS, 6, p. 1-13 (Art N° 28115).

DOI: 10.1038/srep28115
Handle: http://hdl.handle.net/1942/22717

A proposed integrated approach for the preclinical evaluation ofphage therapy in Pseudomonas infections Link
Peer-reviewed author version

Reference (Published version):
Danis-Wlodarczyk, K.; Vandenheuvel, D.; Jang, H.B.; Briers, Y.; Olszak, T.; Arabski, M.; Wasik, S.; Drabik, M.; Higgins, G.; Tyrrell, J.; Harvey, B.J.; Noben, Jean-Paul; Lavigne, R. & Drulis-Kawa, Z.(2016) A proposed integrated approach for the preclinical evaluation ofphage therapy in Pseudomonas infections. In: Scientific Reports, (Art N° 28115)

DOI: 10.1038/srep28115
Handle: http://hdl.handle.net/1942/22501

A proposed integrated approach for the preclinical evaluation of phage therapy in *Pseudomonas* infections.

Katarzyna Danis-Wlodarczyk[1,2], Dieter Vandenheuvel[2], Ho Bin Jang[2], Yves Briers[2, 3], Tomasz Olszak[1], Michal Arabski[4], Slawomir Wasik[5], Marcin Drabik[5], Gerard Higgins[5,6], Jean Tyrrell[7], Brian J. Harvey[7], Jean -Paul Noben[8], Rob Lavigne[2*], Zuzanna Drulis-Kawa[1*]

[1]Department of Pathogen Biology and Immunology, Institute of Genetics and Microbiology, University of Wroclaw, Wroclaw, Poland

[2]Laboratory of Gene Technology, KULeuven, Leuven, Belgium

[3]Laboratory of Applied Biotechnology, Department of Applied Biosciences, Ghent University, Ghent, Belgium

[4] Department of Microbiology, Institute of Biology, The Jan Kochanowski University in Kielce, Kielce, Poland

[5]Department of Molecular Physics, Institute of Physics, The Jan Kochanowski University in Kielce, Kielce, Poland

[6]National Children Research Centre, Dublin, Ireland

[7]Department of Molecular Medicine, Royal College of Surgeons in Ireland, Education and Research Centre, Beaumont Hospital, Dublin, Ireland

[8]Biomedical Research Institute and Transnationale Universiteit Limburg, School of Life Sciences, Hasselt University, Diepenbeek, Belgium

*Corresponding author.

Email: zuzanna.drulis-kawa@uwr.edu.pl (ZDK)

Email: rob.lavigne@kuleuven.be (RL)

Abstract

We implemented several preclinical approaches to assess bacteriophage efficacy against *Pseudomonas* biofilms and infections. Laser interferometry and profilometry were applied to measure biofilm matrix permeability and surface geometry changes, respectively. These biophysical approaches were combined with an advanced Airway Surface Liquid infection model, which mimics *in vitro* the normal and CF lung environments, and an *in vivo Galleria* larvae model .

KTN4 (279,593 bp dsDNA genome) is a type-IV pili dependent, giant phage resembling phiKZ. Upon contact, KTN4 immediately disrupts the *P. aeruginosa* PAO1 biofilm and reduces pyocyanin/pyoverdin production. The gentamicin exclusion assay on NuLi-1 and CuFi-1 cell lines revealed the decrease of extracellular bacterial load between 4 and 7 logs and successfully prevents wild-type *Pseudomonas* internalization into CF epithelial cells. These properties and the significant rescue of *Galleria* larvae indicate that giant KTN4 phage is a suitable candidate for *in vivo* phage therapy evaluation for lung infection applications.

Keywords: giant bacteriophage, *Pseudomonas aeruginosa*, biofilm, Airway Surface Liquid Infection model

Introduction

Pseudomonas aeruginosa is a metabolically versatile Gram-negative bacterium that can cause a wide range of opportunistic hospital-acquired infections. Individuals with open wounds, cancer, compromised immune systems and chronic pulmonary conditions, such as cystic fibrosis (CF) are particularly susceptible (Lyczak et al. 2000; Schroeder et al. 2001; Trautmann et al. 2005). *P. aeruginosa* can undergo phenotypic and genotypic changes in response to the environmental signals during infection and lives as planktonic cells, colonies or biofilms (Bragonzi et al. 2009). The increasing frequency of multidrug-resistant strains is particularly concerning as treatment options are severely limited in the absence of effective antibiotics (Breidenstein et al. 2011; Poole 2011). There is a general need to establish novel strategies for the development of new antibacterial treatments or effective prophylactics as well as new diagnostic tools to identify CF pathogen virulence determinants. One of the possibilities is bacteriophages, the natural parasites of bacteria. Phage cocktails have been applied as alternative or as supportive treatments simultaneously with antibiotics for *P. aeruginosa* eradication causing various infection such as purulent wounds, septicemia, urinary tract or lung infections (Sulakvelidze et al. 2001; Wright et al. 2009; Dorotkiewicz-Jach et al. 2015). Many studies have presented phage high bactericidal effect against CF isolates taken from different stage of infection, reducing the lung bacterial burden in *in vitro* and *in vivo* models (Debarbieux et al. 2010; Morello et al. 2011; Alemayehu et al. 2012; Saussereau et al. 2014; Cullen et al. 2015). Bacterial biofilm eradication is an important aspect towards successful *in vivo* treatments. To overcome the biofilm barrier, phages as evolutionary partners of their hosts have developed specific strategies such as production of highly specific enzymes like polysaccharide depolymerases or alginate lyases. These enzymes allow the phages to invade the bacterial cells entrapped in the polysaccharide backbone by degradation of biofilm structure. Moreover, the bacteria released from exopolysaccharide matrix, become accessible for antimicrobials or host

immune system components (Bayer et al. 1992; Alkawash et al. 2006; Drulis-Kawa et al. 2012; Danis-Wlodarczyk et al. 2015; Olszak et al. 2015). The phiKZ-like phages and their gene products may play an important role in control of pathogenic pseudomonads (Miroshnikov et al. 2006; Briers et al. 2008). Some of these phages have already been incorporated into traditional phage therapy cocktails and continue to be examined for novel therapeutic applications (Matinkhoo et al. 2011; Golshahi et al. 2011; Drulis-Kawa et al. 2014). *Phikzvirus* constitute a genus of 'jumbo' myoviruses, lytic against a variety of *Pseudomonas* species (Krylov et al. 2007; Lavigne et al. 2009). To date, over twenty phiKZ-related phages have been found in soil, water, therapeutic phage preparations, and phage typing schemes from diverse geographic locations (Krylov et al. 2007). PhiKZ-related phages have a large icosahedral head (~122 nm in diameter) and a long (~190 nm) contractile tail surrounded by fibers. Inside the capsid a large cylindrical "inner body" (15–20 MDa, consisting of at least six different proteins), holds the genomic DNA (Krylov et al. 1984; Thomas et al. 2012). This long conserved head component spanning the whole giant capsid wall-to-wall was observed in phiKZ-related phages, e.g. 201 φ2-1, φPA3, EL, OBP (Krylov et al. 2007). Their genomes are very large (between 211 and 317 kb of non-redundant sequence) and compose of circularly permuted, terminally redundant linear double-stranded and A+T-rich (>52%) DNAs (Sokolova et al. 2014) .

This work describes the genome organization and biology of a novel phiKZ isolate KTN4, and its antibacterial potential is examined using novel biofilm assays (interferometry and profilometry) as well as a novel Airway Surface Liquid model on nonCF and CF epithelial cells lines, in an effort to mimic *in vivo* conditions as closely as possible. Indeed, the lung airway surface is covered with a thin airway surface liquid called the ASL, which consists of a mucus layer and a periciliary liquid layer. The former traps and removes inhaled pathogens, while the latter keeps the mucus at an optimal distance from the underlying epithelia to maximize ciliary

mobility, provides a low viscosity solution and acts as a lubricant layer for mucus transport. Together, they play a critical role in effective mucociliary clearance of the airway (Matsui et al. 1998; Zabner et al. 2003). In the case of CF airways due to the decreased ASL volume or altered mucus, bacterial elimination by phagocytes is defective, inflammatory response is abnormal, and mucociliary clearance is reduced. CF airways have a sticky mucus providing the perfect milieu, microaerophilic to anaerobic environment, enabling the colonization and propagation of *P. aeruginosa* (Worlitzsch et al. 2002).

Results and Discussion

Isolation and morphology

Lytic phage KTN4 was isolated from sewage samples collected from irrigated fields located in Wroclaw, Poland. After purification phage titres were 10^{10}- 10^{11} pfu/ml and caused ~ 1.7 mm wide clear plaques with halo zone on 0.6% soft agar. The KTN4 morphology was examined by transmission electron microscopy (TEM) and classified to the *Phikzlikevirus*, order *Caudovirales*, family *Myoviridae* (Fig. S1) (Lavigne et al. 2009). The isolate was formally named vB_PaeM_KTN4 (KTN4). The isometric head size can be estimated at 130 nm between opposite apices, the tail and base plate is 168 nm long.

Molecular analysis and taxonomic context

Genome sequence analysis revealed KTN4 as a giant phage of 279,593 bp, highly similar (>99% genome-wide DNA homology, conserved regulatory elements and genome organisation) to *Pseudomonas* phage phiKZ. A detailed genome and proteome analysis is provided within a dedicated supplementary section, showing minor differences to phiKZ (Suppl.1, Table S1, Fig. S2-S4). An experimental structural proteome analysis (ESI-MS/MS) allowed the identification of 111 virion-associated gene products (out of 368 predicted open reading frames in total). To place this phage into its broader taxonomic context, a protein

sharing network, comprising 495 *Caudovirales* and unclassified phages with 6,948 relationships (edges) between them, was generated (Fig. 1). As expected, phage KTN4 was placed in a single component with five well-known *Pseudomonas* phiKZ-related phages including phiKZ, phiPA3, 201phi2-1, EL and OBP (Cornelissen et al. 2012), as well as four other phages phiJM-2012, SPN3US, CR5, and phiEaH2, which was separated from other components.

One-step growth and stability tests

One-step growth experiments indicated a latent period of 40 min and a burst size of about 6-8 phage particles per infected bacterial cell. The stability test revealed that KTN4 is relatively stable in a broad range of temperature and pH. No reduction of pfu/ml was observed over a period of 60 min at a temperature of 40-70°C, while 1 hour incubation at 80°C and 15 min incubation at 90°C decreased the titer with 4 and 6 log, respectively. After 1 hour incubation at room temperature at pH between 6 and 12 over 90% phages remained infective. At a pH of 3-4 around 10% of particles showed the lytic activity, while pH 2 reduced the titer to less than 1%. No significant change in KTN4 titer was observed after 50% chloroform treatment for 1h incubation at room temperature and at 4°C.

Determination of phage receptor and host range

In the study based on PAO1 mutants it was observed that KTN4 requires the presence of IV type pili on the surface of the host cell as its receptor (Table 1). The lytic activity of KTN4 was examined on two independent *P. aeruginosa* panels. First, 43 clinical *P. aeruginosa* strains from COST international reference panel were used (De Soyza et al. 2013). The KTN4 phage was able to infect 32.6% isolates, compared to representatives of the N4-like group (LUZ7 41.9%), the phiKMV-like group (LUZ19 44.2%), the PB1-like group (LBL3 39.5%, KT28 27.9%, KTN6 41.9%), the phiKZ-like group (phiKZ 46.5%) and a novel jumbo phage PA5oct 23.9%. Second, phage KTN4 exhibited a broad spectrum of activity against 58 clinical strains

from Military Hospital Neder-Over-Heembeek, Brussels, Belgium (Pirnay et al. 2002). KTN4 was able to infect 46.6% strains, whereas representatives of the N4-like group (LUZ7 34.5%, LIT1 12.1%), LUZ24-like group (LUZ24 22.4%), phiKMV-like group (LUZ19 39.7%, LKD16 31.0%, LKA1 3.5%, KMV 32.7%), and PB1-like group (LBL3 46.6%, LMA2 24.1%, LSL4 17.2%, KT28 58.6%, KTN6 67.2%) mostly show a more narrow spectrum (Table S2).

Phage influence on biofilm characteristics covering Nephrophane membrane

The anti-biofilm activity of giant phage KTN4 was evaluated by spectrophotometry and fluorescence assay, and compared with the efficacy of colistin, an anti-pseudomonal drug (Fig 2). The activity of colistin was first adjusted on 24 h PAO1 biofilm growing in microtiter plates and the biofilm mass was evaluated by CV staining. Based on the above results, a concentration of 100 µM colistin was selected (Fig 2A). Afterwards, experiments were performed on the PAO1 biofilm grown on a Nephrophane membrane for three time periods (24, 48 and 72 h). In the Fig 2B, the CV staining of biofilm biomass eradication showed significant effect of active KTN4 and colistin combined with active phage against 72 h-old biofilm. The colistin alone significantly reduced the biomass of the biofilm formed for 24 h. In contrast, the CV assay showed an increase of biomass after intact phage particles treatment of 24 h biofilm. No biofilm mass eradication was noticed for inactivated phages regardless of biofilm age and the combination with colistin. In general, the CV staining did not reveal efficient eradication results both for phage and antibiotic. As discussed recently (Danis-Wlodarczyk et al. 2015), the CV assay has specific limitations. As a consequence, other methods have been applied to evaluate phage potency to affect biofilm forming bacteria. For this purpose, the analysis of pyocyanin and pyoverdin secretion to the medium by spectrophotometry and fluorometry was used, allowing detection of highly diffusible pigmented signaling molecules levels of quorum

sensing and a siderophore (Hassett et al. 1992; Meyer et al. 1996; Allen et al. 2005; Dietrich et al. 2006).

The analysis of pyocyanin concentration in growth medium showed that active phages, colistin and active phage/colistin treatment significantly decreased the level of this compound for the tested biofilms (24, 48 or 72 h) compared to UV-inactivated phages (Fig. 2C). It turned out that infective form of giant phage significantly reduced the concentration of pyocyanin, whether combined with colistin or alone. The level of pyoverdin determined by the fluorescence was significantly lowered after colistin application on 24 h biofilm and in combination with both phage preparations on PAO1 biofilm formed for 72 h (Fig. 2D). The reduction of siderophore concentration was noted also in case if 72 h biofilm exposed to active KTN4. The combined treatment composed of phage and antibiotic did not show a synergistic effect in either biomass or dyes determination assays. This observation is consistent with previous observations for two *Pseudomonas* PB1-like phages (Danis-Wlodarczyk et al. 2015). Moreover, the positive correlation between bacterial cells growth, biofilm formation, pyocyanin and pyoverdin levels in supernatants has been found, indicating that the reduced levels of *Pseudomonas*-specific dyes could be related to phages activity. Statistically significant ($p < 0.005$) inhibition observed for pyocyanin and pyoverdin production was elicited by phages (lysis of cells in biofilm). The quantities of the most important pigmented signaling molecules secreted by the pathogen decreased significantly, which proves the potency of these phages to be applied in *Pseudomonas* biofilm treatment.

The phage application effect on biofilm disruption was analyzed by laser interferometry assay (Arabski et al. 2007; Danis-Wlodarczyk et al. 2015), a biophysical technique measuring the quantitative changes in biofilm matrix permeability for low molecular compounds (Fig. 3). This experiment was not performed for colistin, since no activity of the drug for three-days biofilm could be measured. The diffusion of TSB medium though biofilm was evaluated, which

indirectly indicated its structure degradation. The hydrophilic Nephrophane membrane overgrown by 72 h biofilm was chosen for the interferometry analysis. The PAO1 biofilm was treated with active and UV-inactivated KNT4 phage for 4 h. The diffusion rate of medium transported though the biofilm-covered membrane (0.86×10^{-3} mg/h) was significantly higher than for intact biofilm ($p < 0.001$) after active and inactivated phage treatment, reaching 1.65×10^{-3} mg/h and 1.39×10^{-3} mg/h, respectively. The increase of diffusion rate through the overgrown membrane after phage application indicated the degradation of the biofilm structure associated with the disintegration of matrix elements. It should be emphasized that the increase of the diffusion was also obtained after the application of inactivated particles, suggesting that tested phages are probably equipped with exopolysaccharide depolymerases, responsible for phage particle spread within the biofilm matrix.

The effect of KTN4 phage treatment on biofilm disruption was also analyzed by ZETA-20 non-contact optical profiler, a novel 3D measurement technique. Two of the system imaging modes (Z-Dot™ and Nomarski (ZIC)) were used to determine the 3D profile of tested surface with the reflection on natural colors (Fig. 4). The yellow color of PAO1 biofilm (Fig. 4B) formed on the grey Nephrophane membrane was associated with the production of pyoverdine by bacterial cells leaving in a mature biofilm. After the incubation with KTN4 phage, the color of degraded biofilm was similar to native membrane. It indicated that phage was able to inhibit the production of pyoverdine by PAO1 cells. Moreover, several parameters of surface roughness was also measured what allowed to analyze the physical changes in the biofilm geometry (Table S3). The surface structure, described by Rsk parameter, has changed after incubation with phage preparation. The biofilm surface was smoother after phage treatment observed as the skewness parameter (Rsk) decreased.

Considering anti-biofilm assays in general, it seemed that comparing to CV assay, the novel approaches such as laser interferometry and profilometry (ZETA-20, Zeta Instruments Co., San

Jose, USA) turned out to be more efficient and precise techniques, providing important insights on the degradation and permeability feature of biofilm matrix, and surface geometry changes including several roughness (R) parameters and diffusible pigmented signaling molecules production by biofilm forming bacteria.

Antibacterial efficacy of KTN4 phage analyzed in gentamicin exclusion assay on Airway Surface Liquid infection model

In our study, *in vitro* antibacterial activity of KTN4 phage was assessed in gentamicin exclusion assay on ASL, which is to our knowledge, the first report showing phage treatment efficacy in that infection model. For experiments, two cell lines were selected: 1) NuLi-1 derived from normal human bronchial epithelium and 2) CuFi-1 derived from CF patient bronchial epithelium with significantly thinner ASL (Zabner et al. 2003). Three *P. aeruginosa* strains were selected for these experiments: PAO1 reference strain (piliated, motile strain, effective biofilm former), a nonCF0038 isolate from burn wound (highly expressing type IV pili), both reflecting CF early colonizing isolates, which are non-mucoid with typically smooth LPS and more virulent. The third strain was CF708 from late infection phase, presenting slowly growing and less virulent small colony variants (SCVs) with low expression of type IV pili, and biofilm formation (Olszak et al. 2015). First, both epithelial cell lines were infected with selected strains for 3h and colony count showed *P. aeruginosa* efficiently propagated in both ASLs (10^7-10^9 cfu/ml) (Fig. 5). PAO1 and nonCF0038 pathogens grew better on NuLi-1 cell line, reaching around 1 log higher compared to CuFi-1 ASL. The small colony variant CF708 grew equally well in both types of mucus layer. In the second step of experiment, the KTN4 phage eradication ability of the extracellular bacterial load was evaluated. CFU counts of *P. aeruginosa* were significantly ($p < 0.05$) reduced for the normal NuLi-1 epithelia cells. A 7 log, 6 log and 4 log decrease was observed for PAO1, nonCF0038 and CF708, respectively (Fig. 5A). In the case of the CuFi-1 epithelia the phage treatment was also very effective giving 4 log, 6 log and 5 log

reductions in colony count of PAO1, nonCF0038 and CF708, respectively (Fig. 5A). PAO1 was significantly more susceptible ($p < 0,05$) to phage treatment in NuLi-1 cells compared to CuFi-1 cells, contrary to the CF708 isolate. It was confirmed that the KTN4 phage could freely diffuse and gain access to the bacterial hosts in both ASL models, but the final result of the treatment was strongly dependent on the strain features or due to different ASL pH between NuLi-1 and CuFi-1 cells. A possible explanation of this phenomenon was observed by Worlitzsch's studies (Worlitzsch et al. 2002) where *P. aeruginosa* was not interacting with the CF epithelium directly, but was rather found trapped in mucus plugs formed in the airways. Thus, the phage receptors could be masked by mucus elements, which have an influence on phage adsorption to bacterial cell surface. Moreover, the CF strain better adapted to CuFi-1 environment could probably express more efficiently the type IV pili, which are receptors for KTN4 phage.

In the next step of our experiment, the ability of *P. aeruginosa* strains to invade into epithelial cells was investigated (Fig. 5B). Although *P. aeruginosa* was generally thought to be an extracellular pathogen, a number of different groups have found that it can be internalized into a range of different cell types, including epithelial cells (Fleiszig et al. 1995; Schroeder et al. 2001). The results showed that CF and nonCF strains could indeed internalize into both cell lines and no statistically significant differences were observed for all pathogens. The PAO1 and nonCF0038 were much less ingested by epithelium compared to the CF708 isolate, where only 4.50E-05% and 2.00E-04 – 5.00E-05% of infecting population were able to internalize into NuLi-1 and CuFi-1 cells, respectively, in contrast to 0.05% and 0.06% for CF708 isolate. Clearly the internalization capability and adaptations of CF708 strain were more effective compared to the nonCF strains, consistent with previous observations (Fleiszig et al. 1995). This suggests that the *Pseudomonas* strains with high cytotoxicity are low invasive and vice

versa, bacteria less virulent enter the epithelial cells to survive intracellularly without killing the host cell.

In the last step, the influence of KTN4 phage treatment on the number of invaded bacteria was evaluated (Fig. 5B). In the NuLi-1 cell line there were no significant changes in CFU counts for all *P. aeruginosa* invading strains after phage application. A possible explanation is that during the 3 hours of pretreatment, all bacterial cells were already internalized, thus the phage had no access to these host cells. In contrast, the phage application was significantly more effective for CuFi-1 internalization prevention by wild type *P. aeruginosa* strains, since CF lung cells due to lack of CFTR, show significantly less ingestion rate of LPS-smooth bacteria and significantly greater lung burdens post-infection than wild-type epithelium (Schroeder et al. 2001). As previously mentioned (Worlitzsch et al. 2002)), wild strains not well adopted to sticky and dense CF environment are absent on epithelial surface but remain as macrocolonies within intraluminal material, slowing down efficient internalization. Simultaneously, phage application cause effective eradication of bacterial cells trapped in the mucus plugs. The CF708 isolate evolving in CF patient is able to internalize with the CuFi-1 epithelium in relatively short time after infection evading phage lytic activity.

Antibacterial efficacy of KTN4 phage analyzed *in vivo* on wax moth larvae model

The wax moth larvae model has been chosen for the *in vivo* assay because the *P. aeruginosa,* as a natural *Galleria* pathogen, is highly virulent in these insects when inoculated directly into the hemolymph (Miriagou et al. 2010; Fancello et al. 2011). The lethal dose causing fast infection progress was established as follows: 10 CFU for PAO1 and nonCF0038 strains and 10^6 CFU of CF708 isolate per larvae and the treatment was carried out by the injection of phage lysate at multiplicity of infection (MOI) of 100 (Fig. 6). The negative controls (uninfected and receiving phage lysate larvae) gave a 100% survival rate. The 10 CFU of PAO1 and

non-CF0038 strains caused 100% caterpillar mortality after one day of infection. The small colony variant CF708 isolate even at very high inoculum (10^6 CFU) was significantly less virulent than former ones ($p < 0.0001$) with the delay of killing 20% and 40% after three and four days of infection, respectively.

The KTN4 phage application showed a significant impact on *Galleria* larval survival rate from lethal PAO1 infection rescuing 90% of caterpillars 36 h post injection ($p < 0.0001$). The protective activity of the phage against nonCF0038 propagation was much less efficient saving only 20% of larvae at the same time ($p < 0.0001$). The antibacterial activity of applied phage against CF708 isolate was seen at the very end of the experiment (fourth day) with 90% survival rate of treated larvae in comparison to 60% of untreated control.

The results obtained in *G. mellonella* model generally correlated with data observed for NuLi-1 cells in ASL infection assay, where the bacterial count of PAO1 was reduced by KTN4 phage more efficiently than of non-CF0038 strain, although the later one was assigned as a strong type IV pili former (a receptor of KTN4 phage). The possible explanation of this effect could be the biochemical clonally variation of non-CF308 population examined by Fourier transform infrared spectroscopy (FTIR) analysis in the spectra window of carbohydrates and lipids, in our previous study (Olszak et al. 2015). This may influence the stronger variation of phage susceptible cells among treated non-CF308 population. Comparing presented *Galleria* experiment to our previous study done on the same strains (Olszak et al. 2015), the protective efficacy ($p < 0.0001$) of KTN4 phage was similar to the activity of another giant phage PA5oct tested in Olszak et al. study, which rescued 90% of caterpillars after two days of PAO1 infection. The increased larval survival rate in the presence of PB1-like phage (100% at the same time) compared to the giants ones, could suggest the importance of phage size and phage generation time rate (KT28 < PA5oct and KTN4) in the therapeutic results (Olszak et al. 2015).

In the moth larvae model an antibacterial potential of KTN4 phage was proven against *P. aeruginosa* pathogen. Nevertheless, the administration of bacteriolytic agent (antibiotic, phage) in the treatment of infection, especially caused by Gram-negative bacteria, may result in severe consequences as Systemic *Inflammatory* Response Syndrome. The rapid release of lipopolysaccharide (LPS) during lysis of a big number of cells in a short period of time, may leads to serious side effects in treated patient, thus the therapy should be carefully selected.

Conclusions

Genome and proteome analysis, as well as a protein-sharing network indicates that KTN4 phage belongs to "jumbo" *Myoviridae* and it is closely related to phiKZ phage. This lytic virus has a broad spectrum of activity with prevalence to clinical isolates, especially from CF patients. Moreover, this phage has a very strong bactericidal effect (4-7 log reduction of colony count) against *P. aeruginosa* strains, as tested in a ASL model. To our knowledge this is the first study of phage application using this lung epithelia infection assay. The gentamicin exclusion assay on ASL *in vitro* model is flexible, generates reproducible data with well-controlled and standardized conditions, mimicing the normal and CF lung environments. Moreover, it provides a basis for understanding the host-pathogen interactions and is, as such, an important step towards experimental *in vivo* studies. Indeed, the *Galleria* larvae model provides a first confirmation of the *in vivo* potential of the antibacterial efficacy of KTN4 phage against clinical isolates, albeit in a strain dependent manner.

Since *Pseudomonas* common infections are usually associated with biofilm formation, the ability of KTN4 to disrupt the biofilm has been examined in detail. The phage demonstrated a strong anti-biofilm potential immediately after application. In contrast to the commonly used CV assay, novel biophysical techniques (interferometry and profilometry) have proven to be sensitive and reproducible techniques, providing information on changes in biofilm permeability and the 3D structure, during the biofilm structure degradation process.

Considering all these characteristics, KTN4 phage is a suitable and promising candidate for *in vivo* trials, for applications in treatment and prophylaxis in lung infections.

Materials and Methods

Isolation, propagation and purification of phages

The *Pseudomonas aeruginosa* PAO1 (ATCC 15692) strain was used as phage propagation host. Environmental water samples from irrigated fields in Wroclaw, Poland were centrifuged (15,000 g for 15 min) and the supernatant was filtered through a 0.22 µm Millex-GP filter (Merck Millipore, Germany) to remove bacterial debris. *Pseudomonas* phage KTN4 has been propagated as previously described (Danis-Wlodarczyk et al. 2015). Phage lysate was purified with CsCl-gradient ultracentrifugation as described by Ceyssens *et al.* (Ceyssens et al. 2008). The phage titre of the solution was assessed using the double-agar layer technique (Adams 1959). The virion morphology in transmission electron microscopy (TEM) was established according to the method described elsewhere (Danis-Wlodarczyk et al. 2015).

DNA isolation and sequencing

Phage DNA was isolated according to the modified protocol for λ DNA isolation (Ceyssens et al. 2009) after CsCl gradient purification of phage particles (10^{10} pfu/ml). Whole genome sequencing was performed by use of the Illumina MiSeq platform available at the Nucleomics Core (VIB, Belgium). A 2*150 bp paired-end library (Nextera XT sample prep) was prepared and sequenced. The reads were assembled in a single contig with a 100-6000 fold coverage using CLC genomics Workbench *de novo* assembly algorithm (CLC bio, Qiagen Company). The genome of bacteriophage KTN4 was deposited at GenBank under accession number KU521356.

In silico genome analysis

Potential ORFs were identified using the GeneMark S (Besemer et al. 2001), GeneMark.hmm (Lukashin and Borodovsky 1998), OrfFinder (Sayers et al. 2011) and manually analyzed. Translated ORFs were compared to known proteins using BLASTP (Altschul et al. 1990), the HHpred server (Söding et al. 2005) and HMMER (Finn et al. 2011), providing further insight into the predicted function of proteins. Conserved protein domains were identified using the Pfam (Finn et al. 2006), InterPro (Mitchell et al. 2014) and PHYRE2 (Kelley et al. 2015). Putative tRNA genes were searched for using the tRNAscan-SE program (Lowe and Eddy 1997). The intergenic regions were screened for regulatory elements using fuzznuc (Rice et al. 2000) and manually evaluated. Putative factor-independent terminators were identified with ARNOLD software (Naville et al. 2014).

Protein family clustering and network construction and analyses

To represent the genetic relationships of KTN4 with other phages as a gene (protein)-sharing network, each predicted protein was clustered into protein families using the ACLAME database (version 0.4) (Leplae et al. 2010) with the database of "viruses" and an E-value <0.001 (Lima-Mendez et al. 2008). Additionally, for the phages that share significant gene contents with KTN4 but are absent in the ACLAME database, 2,592 protein sequences were retrieved from phiKZ (NC_004629), phiPA3 (HQ630627), 201phi2-1 (NC_010821), EL (NC_007623), OBP (NC_016571), phiJM-2012 (JQ340088), SPN3US (NC_027402), CR5 (NC_021531), and phiEaH2 (NC_019929). The proteins that could not be assigned into any ACLAME protein families were defined as the unclassified protein families (UPFs) as previously described (Jang et al. 2013a). We accepted the transitive nature of sequence families (Casjens 2003), i.e., a sequence is added to a cluster if it shares a reciprocal best hit relationship with at least one of the sequences of the cluster. The degree of similarity between other phages was generated as the minus logarithmic score by multiplying hypergeometric similarity *P*-value by the total

number of pairwise comparisons (Lima-Mendez et al. 2008). Afterwards, a protein-sharing network was built with the Cytoscape software platform (version 3.1.1; http://cytoscape.org/), using an edge-weighted spring embedded model. Topological properties of the network were estimated with the Network Analyzer 2.7 Cytoscape plug-in (Brohée et al. 2008).

ESI-MS/MS analysis of structure-associated proteins

Phage proteins were extracted from a purified phage suspension (10^{11} pfu/ml) by a single methanol/chloroform extraction (1:1:0.75, v/v/v) (Acros Organics) and subsequently precipitated by addition of an equal volume of methanol (16,060 *g*, 6 min). The dried phage protein pellet was resuspended in SDS-PAGE loading buffer and boiled for 5 min before loading onto a 12% SDS-PAGE gel. Protein gels were stained afterwards with GelCode Blue Safe (Thermo Scientific). Further, the entire lane of a phage protein profile was prepared for ESI- MS/MS as previously described (Ceyssens et al. 2014; Van den Bossche et al. 2014).

Burst size experiments and Sensitivity of phage particles to heat, chloroform and pH

A one-step growth curve was performed according to the method of Pajunen *et al.* (Pajunen et al. 2000) with modifications. An equal volume of bacterial culture (at optical density at 600 nm of 0.4) was mixed with phage suspension (10^6 pfu/ml) to obtain a multiplicity of infection of 0.01. Phages were allowed to adsorb for 8 min at 37 ºC, after which the mixture was diluted to 10^{-4}. Triplicate samples were taken during 1 h at 5 min intervals and titrated. The sensitivity of phage particles to heat, chloroform and pH were performed according to previously described methods (Danis-Wlodarczyk et al. 2015).

Phage typing and phage receptor analysis

The lytic activity of KTN4 was examined on 58 clinical strains from Military Hospital Neder-Over-Heembeek, Brussels, Belgium collection (Pirnay et al. 2002) for comparison to other

Pseudomonas phages including: N4-like group (LUZ7, LIT1), LUZ24-like group (LUZ24), phiKMV-like group (LUZ19, LKD16,LKA1, KMV), PB1-like group (LBL3, LMA2, LSL4, KT28, KTN6) (Table S3). Moreover, the phage specificity to particular bacterial receptor was tested on PAO1 mutants deficient in biosynthesis of A-band and B-band O-antigen, flagella, IV type pili, or alginate production (Table 1). For all phage experiments 4-6 h old bacterial cultures were used, unless otherwise stated. To determine bacterial susceptibility to phage-mediated lysis, a drop of the phage suspension (10^8 pfu/ml) was put on a bacterial lawn and incubated at 37ºC. The plates were checked after 4-6 h and again after 18 h for the presence of a lysis zone (Kutter 2009).

Phage influence on biofilm characteristics covering Nephrophane membrane

Nephrophane (VEB Filmfabrik, Wolfen, Germany) is a microporous, highly hydrophilic membrane made from cellulose acetate ([trio-acetate cel-(OCO-CH3)n]) of a spongy structure (Arabski et al. 2007; Wąsik et al. 2015). The analysis of biofilm degradation by intact and UV-inactivated phages was performed by microbiological methods as well as biophysical techniques. In the first step of the study, the antibacterial effect of colistin against PAO1 biofilm formed in TSB medium for 24 h at 37°C was determined. This step was made in microtitre plates using the CV (0.004% crystal violet) assay. Afterwards, the Nephrophane membrane was covered by a PAO1 biofilm formed for either 24, 48 or 72 h at 37°C in TSB medium. Next, the biofilm was treated for 4 hours with KTN4 phage (5×10^8 pfu/ml) and/or colistin at a 100 µM concentration at 37°C. After incubation, the biofilm was stained with CV (0.004%) for 15 min or was tested for pyocyanin and pyoverdin levels in the supernatants, as previously described (Danis-Wlodarczyk et al. 2015). The degradation of biofilm by phages is associated with increase of the permeability of its matrix for low molecular compounds. The quantitative measurements of cultivation medium (TSB) diffusion through biofilm structure after incubation

with phages might indicate on disruption of its structure. This degrading activity of KTN4 phage on PAO1 biofilm was tested by laser interferometry method as presented elsewhere (Arabski et al. 2007; Danis-Wlodarczyk et al. 2015). The level of Nephrophane membrane covered by biofilm was determined as 92.4% . The interferometry system consisted of two glass cuvettes, separated by the horizontally located Nephrophane membrane, covered with PAO1 biofilm formed for 72 h at 37°C. The KTN4 phage treatment (5×10^8 pfu/ml) was carried out for 4 h at 37°C. All experiments were performed in triplicate.

PAO1 biofilm surface geometry, its physical parameters as well as true color of 3D optical profile were determined by ZETA-20 (Zeta Instruments Co., San Jose, USA). Two imaging modes, Z-Dot™ Optical Profiler and Nomarski (ZIC), were applied. Measurements were made for 188 µm × 141 µm areas with a resolution 0.046 µm in the Z axis. Several roughness (R) parameters were defined: Ra – arithmetical mean deviation, Rq – root mean square deviation, Rp – maximum profile peak height, Rv – maximum profile valley depth, Rsk – skewness, Rz – maximum height of profile, and Rku – kurtosis of profile. For each of these parameters the value minimum, maximum, mean, standard deviation and relative error has been determined.

Gentamicin exclusion assay on Airway Surface Liquid infection model

NuLi-1 (Normal Lung, University of Iowa), derived from human airway epithelium of normal genotype, and a CF cell line, called CuFi-1 (Cystic Fibrosis, University of Iowa), derived from bronchial epithelium of a homozygous CFTR F508del/F508del individual, were kindly provided by Zabner (University of Iowa, Iowa City, IA). The ASL model was prepared according to methods described elsewhere by Zabner (Zabner et al. 2003). Both cell lines were inoculated with 25µl of *P. aeruginosa* PAO1 reference strain (6.2×10^7 cfu/ml), nonCF0038 isolate from burn wound (6.5×10^7 cfu/ml) and CF708 small colony variant (1.0×10^6 cfu/ml) at optical density at 600 nm of 0.1, and incubated for 1.5 h at 37°C, 5% CO_2. The 25µl of KTN4

phage suspension (8.5×10^{10} pfu/ml) was added to each millicell hanging cell culture insert. Subsequently, cells were incubated for 1.5 h at 37°C, 5% CO_2. Next, cells were washed with PBS and apical washes were serially diluted in DMEM:F12 medium (Sigma-Aldrich) and quantified by viable counts on LB agar (Sigma-Aldrich) after 24 hours. To evaluate the ability of *P. aeruginosa* to invade into epithelial cells and the ability of phage KTN4 to prevent this invasion, extracellular and adherent bacteria were killed by addition of 400µg/ml gentamicin (Thermo-Fisher Scientific) and incubated for 1 h at 37 °C, 5% CO_2. The drug was subsequently removed by PBS washing and epithelial cells were lysed with 0.4% Triton-X100 (Sigma-Aldrich) 100 µl for 15 min at 37 °C, 5% CO_2. The resulting lysate was serially diluted in DMEM:F12 medium and quantified by viable counts on LB agar after 24 hours. The gentamicin MICs for tested strains were as follows: 0.5 µg/ml, 2 µg/ml, and 64 µg/ml, for PAO1, nonCF0038 and CF708, respectively. Several controls of epithelial cells viability were prepared: (i) a negative control without any treatment, (ii) a negative control with TC media; (iii) a positive control with Triton-X100; (iv) 1.5 h after KTN4 treatment; (v) 1,5 h after strains treatment. The Nuli-1 and CuFi-1 cells were stained with 8 µM Calcien AM (live staining) (Life Technologies, NY, USA) and 3 µM propidium iodide (PI) (dead staining) (Life Technologies, NY, USA) according to manufacturer's instructions. Negative controls (untreated) and positive controls (0.25% Triton-X100 treated) were included in the experimental set up. After staining, in all cases, filter inserts were XZ scanned using a confocal microscope (Zeiss LSM 510 Meta 40× objective, Jena, Germany). No toxicity influence of cell lines was noticed for phage and bacteria samples.

Statistical analysis

The data were analyzed using the Statistica software package (StatSoft, Tulsa, OK, USA). All the values were expressed as mean ± SD and significant differences between variations

(denoted p-values < 0.05) were found by means of the Snedecor-Fisher test using one-way ANOVA.

Galleria mellonella larvae model

The *in vivo* assay was conducted on a wax moth larvae model according to the methodology described previously (Olszak et al. 2015). Briefly, larvae were inoculated with 10 µl lethal dose of bacterial cells established as follows: 10 CFU of PAO1 and nonCF0038 strains and 10^6 CFU of CF708 isolate per larvae. After injection into the ventral side of the last pair of pseudopods, the larvae were incubated for 96 hours at 37°C. For assessment of the antibacterial activity of KTN4 phage, larvae were sequentially injected with 10 µl of bacterial suspension and 10 µl of phage lysate at the titration equal to multiplicity of infection (MOI) 100. The results were read at 18, 24, 36, 48, 72 and 96 hours post injection and were expressed as the percentage survival rate assessed by macroscopic appearance. Experiments were performed in triplicate (10 larvae per trial). The controls consisted of uninfected and larvae receiving phage lysate only (negative) and infected with bacterial lethal dose (positive). The analysis of survival curves was performer by log-rank Mantel-Cox test. P-values <0.05 were considered statistically significant. Statistical analysis was performed using GraphPad Prism software (GraphPad Software, Inc., La Jolla, USA).

Acknowledgements

This study was supported by Polish National Science Centre research grant no. 2012/04/M/NZ6/00335. Katarzyna Danis-Wlodarczyk was co-financed by the European Union as part of the European Social Fund. The authors thank Sylwia Nowak (UWR) for excellent technical assistance. We acknowledge Nikos Ekizoglou from Zeta Instruments Co., San Jose, USA, for providing the ZETA-20 profiler used in biofilm surface geometry assay. RL is a member of the “PhageBiotics” research community, supported by the FWO Vlaanderen.

Zuzanna Drulis-Kawa and Brian Harvey are members of the EU COST Action in Microbial cell surface determinants of virulence (http://www.cost.eu/COST_Actions/bmbs/BM1003).

Competing interests

The authors declare that they have no competing interests.

References

Adams MH (1959) Bacteriophages. In: Adams MH (ed) Bacteriophages. Interscience Publishers, New York, pp 27–30

Alemayehu D, Casey PG, McAuliffe O, Guinane CM, Martin JG, Shanahan F, Coffey A, Ross RP, Hill C (2012) Bacteriophages MR299-2 and NH-4 Can Eliminate Pseudomonas aeruginosa in the Murine Lung and on Cystic Fibrosis Lung Airway Cells. MBio 3:e00029–12–e00029–12. doi: 10.1128/mBio.00029-12

Alkawash MA, Soothill JS, Schiller NL (2006) Alginate lyase enhances antibiotic killing of mucoid Pseudomonas aeruginosa in biofilms. APMIS 114:131–8. doi: 10.1111/j.1600-0463.2006.apm_356.x

Allen L, Dockrell DH, Pattery T, Lee DG, Cornelis P, Hellewell PG, Whyte MKB (2005) Pyocyanin production by Pseudomonas aeruginosa induces neutrophil apoptosis and impairs neutrophil-mediated host defenses in vivo. J Immunol 174:3643–3649.

Altschul SF, Gish W, Miller W, Myers EW, Lipman DJ (1990) Basic local alignment search tool. J Mol Biol 215:403–410. doi: 10.1016/S0022-2836(05)80360-2

Arabski M, Wąsik S, Dworecki K, Kaca W (2007) Laser interferometric determination of ampicillin and colistin transfer through cellulose biomembrane in the presence of Proteus vulgaris O25 lipopolysaccharide. J Memb Sci 299:268–275. doi: 10.1016/j.memsci.2007.05.003

Bayer AS, Park S, Ramos MC, Nast CC, Eftekhar F, Schiller NL (1992) Effects of alginase on the natural history and antibiotic therapy of experimental endocarditis caused by mucoid Pseudomonas aeruginosa. Infect Immun 60:3979–3985.

Besemer J, Lomsadze A, Borodovsky M (2001) GeneMarkS: a self-training method for prediction of gene starts in microbial genomes. Implications for finding sequence motifs in regulatory regions. Nucleic Acids Res 29:2607–2618. doi: 11410670

Bragonzi A, Paroni M, Nonis A, Cramer N, Montanari S, Rejman J, Di Serio C, Döring G, Tümmler B (2009) Pseudomonas aeruginosa microevolution during cystic fibrosis lung infection establishes clones with adapted virulence. Am J Respir Crit Care Med 180:138–145. doi: 10.1164/rccm.200812-1943OC

Breidenstein EBM, de la Fuente-Núñez C, Hancock REW (2011) Pseudomonas aeruginosa: all roads lead to resistance. Trends Microbiol 19:419–426. doi: 10.1016/j.tim.2011.04.005

548 Briers Y, Miroshnikov K, Chertkov O, Nekrasov A, Mesyanzhinov V, Volckaert G, Lavigne
549 R (2008) The structural peptidoglycan hydrolase gp181 of bacteriophage phiKZ.
550 Biochem Biophys Res Commun 374:747–751. doi: 10.1016/j.bbrc.2008.07.102

551 Briers Y, Volckaert G, Cornelissen A, Lagaert S, Michiels CW, Hertveldt K, Lavigne R
552 (2007) Muralytic activity and modular structure of the endolysins of Pseudomonas
553 aeruginosa bacteriophages phiKZ and EL. Mol Microbiol 65:1334–1344. doi:
554 10.1111/j.1365-2958.2007.05870.x

555 Brohée S, Faust K, Lima-Mendez G, Vanderstocken G, van Helden J (2008) Network
556 Analysis Tools: from biological networks to clusters and pathways. Nat Protoc 3:1616–
557 1629. doi: 10.1038/nprot.2008.100

558 Casjens S (2003) Prophages and bacterial genomics: What have we learned so far? Mol
559 Microbiol 49:277–300. doi: 10.1046/j.1365-2958.2003.03580.x

560 Ceyssens P-J, Mesyanzhinov V, Sykilinda N, Briers Y, Roucourt B, Lavigne R, Robben J,
561 Domashin A, Miroshnikov K, Volckaert G, Hertveldt K (2008) The genome and
562 structural proteome of YuA, a new Pseudomonas aeruginosa phage resembling M6. J
563 Bacteriol 190:1429–1435. doi: 10.1128/JB.01441-07

564 Ceyssens P-J, Minakhin L, Van den Bossche A, Yakunina M, Klimuk E, Blasdel B, De Smet
565 J, Noben J-P, Bläsi U, Severinov K, Lavigne R (2014) Development of giant
566 bacteriophage ϕKZ is independent of the host transcription apparatus. J Virol 88:10501–
567 10. doi: 10.1128/JVI.01347-14

568 Ceyssens P-J, Miroshnikov K, Mattheus W, Krylov V, Robben J, Noben J-P,
569 Vanderschraeghe S, Sykilinda N, Kropinski AM, Volckaert G, Mesyanzhinov V,
570 Lavigne R (2009) Comparative analysis of the widespread and conserved PB1-like
571 viruses infecting Pseudomonas aeruginosa. Environ Microbiol 11:2874–83. doi:
572 10.1111/j.1462-2920.2009.02030.x

573 Cloutier I, Paradis-Bleau C, Giroux A-M, Pigeon X, Arseneault M, Levesque RC, Auger M
574 (2010) Biophysical studies of the interactions between the phage varphiKZ gp144 lytic
575 transglycosylase and model membranes. Eur Biophys J 39:263–76. doi: 10.1007/s00249-
576 009-0530-1

577 Cornelissen A, Ceyssens PJ, Krylov VN, Noben JP, Volckaert G, Lavigne R (2012)
578 Identification of EPS-degrading activity within the tail spikes of the novel Pseudomonas
579 putida phage AF. Virology 434:251–256. doi: 10.1016/j.virol.2012.09.030

580 Cullen L, Weiser R, Olszak T, Maldonado R, Moreira A, Slachmuylders L, Brackman G,
581 Paunova-Krasteva T, Zarnowiec P, Czerwonka G, Reilly J, Drevinek P, Kaca W, Melter
582 O, De Soyza A, Perry A, Winstanley C, Stoitsova S, Lavigne, R Mahenthiralingam E,
583 Sá-Correia I, Coenye T, Drulis-Kawa Z, Augustyniak D, Valvano M, McClean S (2015)
584 Phenotypic characterization of an international Pseudomonas aeruginosa reference panel:
585 strains of cystic fibrosis (CF) origin show less in vivo virulence than non-CF strains.
586 Microbiology 161:1961–77. doi: doi: 10.1099/mic.0.000155

587 Danis-Wlodarczyk K, Olszak T, Arabski M, Wasik S, Majkowska-Skrobek G, Augustyniak
588 D, Gula G, Briers Y, Jang H Bin, Vandenheuvel D, Duda KA, Lavigne R, Drulis-Kawa
589 Z (2015) Characterization of the Newly Isolated Lytic Bacteriophages KTN6 and KT28
590 and Their Efficacy against Pseudomonas aeruginosa Biofilm. PLoS One 10:e0127603.
591 doi: 10.1371/journal.pone.0127603

592 De Soyza A, Hall AJ, Mahenthiralingam E, Drevinek P, Kaca W, Drulis-Kawa Z, Stoitsova
593 SR, Toth V, Coenye T, Zlosnik JE a, Burns JL, Sá-Correia I, De Vos D, Pirnay J-P, J
594 Kidd T, Reid D, Manos J, Klockgether J, Wiehlmann L, Tümmler B, McClean S,
595 Winstanley C (2013) Developing an international Pseudomonas aeruginosa reference
596 panel. Microbiologyopen 2:1010–23. doi: 10.1002/mbo3.141

597 Debarbieux L, Leduc D, Maura D, Morello E, Criscuolo A, Grossi O, Balloy V, Touqui L
598 (2010) Bacteriophages can treat and prevent Pseudomonas aeruginosa lung infections. J
599 Infect Dis 201:1096–104. doi: 10.1086/651135

600 Dietrich LEP, Price-Whelan A, Petersen A, Whiteley M, Newman DK (2006) The phenazine
601 pyocyanin is a terminal signalling factor in the quorum sensing network of Pseudomonas
602 aeruginosa. Mol Microbiol 61:1308–1321. doi: 10.1111/j.1365-2958.2006.05306.x

603 Dorotkiewicz-Jach A, Augustyniak D, Olszak T, Drulis-Kawa Z (2015) Modern therapeutic
604 approaches against Pseudomonas aeruginosa infections. Curr Med Chem 22:1642–64.
605 doi: 10.2174/0929867322666150417122531#sthash.c9Zwlpw7.dpuf

606 Drulis-Kawa Z, Majkowska-Skrobek G, Maciejewska B, Delattre A-S, Lavigne R (2012)
607 Learning from bacteriophages - advantages and limitations of phage and phage-encoded
608 protein applications. Curr Protein Pept Sci 13:699–722. doi:
609 10.2174/138920312804871193

610 Drulis-Kawa Z, Olszak T, Danis K, Majkowska-Skrobek G, Ackermann H-W (2014) A giant
611 Pseudomonas phage from Poland. Arch Virol 159:567–572. doi: 10.1007/s00705-013-
612 1844-y

613 Fancello L, Desnues C, Raoult D, Rolain JM (2011) Bacteriophages and diffusion of genes
614 encoding antimicrobial resistance in cystic fibrosis sputum microbiota. J Antimicrob
615 Chemother 66:2448–54. doi: 10.1093/jac/dkr315

616 Finn RD, Clements J, Eddy SR (2011) HMMER web server: Interactive sequence similarity
617 searching. Nucleic Acids Res. doi: 10.1093/nar/gkr367

618 Finn RD, Mistry J, Schuster-Böckler B, Griffiths-Jones S, Hollich V, Lassmann T, Moxon S,
619 Marshall M, Khanna A, Durbin R, Eddy SR, Sonnhammer ELL, Bateman A (2006)
620 Pfam: clans, web tools and services. Nucleic Acids Res 34:D247–D251. doi:
621 10.1093/nar/gkj149

622 Fleiszig SM, Zaidi TS, Pier GB (1995) Pseudomonas aeruginosa invasion of and
623 multiplication within corneal epithelial cells in vitro. Infect Immun 63:4072–4077.

624 Fokine A, Miroshnikov K a, Shneider MM, Mesyanzhinov V V, Rossmann MG (2008)
625 Structure of the bacteriophage phi KZ lytic transglycosylase gp144. J Biol Chem
626 283:7242–50. doi: 10.1074/jbc.M709398200

627 Golshahi L, Lynch KH, Dennis JJ, Finlay WH (2011) In vitro lung delivery of bacteriophages
628 KS4-M and ΦKZ using dry powder inhalers for treatment of Burkholderia cepacia
629 complex and Pseudomonas aeruginosa infections in cystic fibrosis. J Appl Microbiol
630 110:106–17. doi: 10.1111/j.1365-2672.2010.04863.x

631 Halary S, Leigh JW, Cheaib B, Lopez P, Bapteste E (2010) Network analyses structure
632 genetic diversity in independent genetic worlds. Proc Natl Acad Sci U S A 107:127–132.
633 doi: 10.1073/pnas.0908978107

634 Hassett DJ, Charniga L, Bean K, Ohman DE, Cohen MS (1992) Response of Pseudomonas

635 aeruginosa to pyocyanin: mechanisms of resistance, antioxidant defenses , and
636 demonstration of a manganese-cofactored superoxide dismutase. 60:328–336.

637 Jang H Bin, Fagutao FF, Nho SW, Park S Bin, Cha IS, Yu JE, Lee JS, Im SP, Aoki T, Jung
638 TS (2013a) Phylogenomic network and comparative genomics reveal a diverged member
639 of the ΦKZ-related group, marine vibrio phage ΦJM-2012. J Virol 87:12866–78. doi:
640 10.1128/JVI.02656-13

641 Jang H Bin, Fagutao FF, Nho SW, Park S Bin, Cha IS, Yu JE, Lee JS, Im SP, Aoki T, Jung
642 TS (2013b) Phylogenomic network and comparative genomics reveal a diverged member
643 of the ΦKZ-related group, marine vibrio phage ΦJM-2012. J Virol 87:12866–78. doi:
644 10.1128/JVI.02656-13

645 Kelley LA, Mezulis S, Yates CM, Wass MN, Sternberg MJE (2015) The Phyre2 web portal
646 for protein modeling, prediction and analysis. Nat Protoc 10:845–858. doi:
647 10.1038/nprot.2015.053

648 Krylov V, Smirnova T, Minenkova I, Plotnikova T, Zhazikov I, Khrenova E (1984)
649 Pseudomonas bacteriophage φKZ contains an inner body in its capsid. Can J Microbiol
650 30:758–62.

651 Krylov VN, Dela Cruz DM, Hertveldt K, Ackermann H-W (2007) “phiKZ-like viruses”, a
652 proposed new genus of myovirus bacteriophages. Arch Virol 152:1955–9. doi:
653 10.1007/s00705-007-1037-7

654 Kutter E (2009) Phage host range and efficiency of plating. Methods Mol Biol 501:141–149.
655 doi: 10.1007/978-1-60327-164-6_14

656 Lavigne R, Darius P, Summer EJ, Seto D, Mahadevan P, Nilsson AS, Ackermann HW,
657 Kropinski AM (2009) Classification of Myoviridae bacteriophages using protein
658 sequence similarity. BMC Microbiol 9:224. doi: 10.1186/1471-2180-9-224

659 Leplae R, Lima-Mendez G, Toussaint A (2010) ACLAME: a CLAssification of Mobile
660 genetic Elements, update 2010. Nucleic Acids Res 38:D57–61. doi: 10.1093/nar/gkp938

661 Lima-Mendez G, Van Helden J, Toussaint A, Leplae R (2008) Reticulate representation of
662 evolutionary and functional relationships between phage genomes. Mol Biol Evol
663 25:762–777. doi: 10.1093/molbev/msn023

664 Lowe TM, Eddy SR (1997) tRNAscan-SE: A program for improved detection of transfer
665 RNA genes in genomic sequence. Nucleic Acids Res 25:955–964. doi:
666 10.1093/nar/25.5.955

667 Lukashin A V., Borodovsky M (1998) GeneMark.hmm: New solutions for gene finding.
668 Nucleic Acids Res 26:1107–1115. doi: 10.1093/nar/26.4.1107

669 Lyczak JB, Cannon CL, Pier GB (2000) Establishment of Pseudomonas aeruginosa infection:
670 lessons from a versatile opportunist. Microbes Infect 2:1051–1060. doi: S1286-
671 4579(00)01259-4 [pii]

672 Matinkhoo S, Lynch KH, Dennis JJ, Finlay WH, Vehring R (2011) Spray-dried respirable
673 powders containing bacteriophages for the treatment of pulmonary infections. J Pharm
674 Sci 100:5197–205. doi: 10.1002/jps.22715

675 Matsui H, Grubb BR, Tarran R, Randell SH, Gatzy JT, Davis CW, Boucher RC (1998)
676 Evidence for periciliary liquid layer depletion, not abnormal ion composition, in the

677 pathogenesis of cystic fibrosis airways disease. Cell 95:1005–1015. doi: 10.1016/S0092-
678 8674(00)81724-9

679 Meyer JM, Neely A, Stintzi A, Georges C, Holder IA (1996) Pyoverdin is essential for
680 virulence of Pseudomonas aeruginosa. Infect Immun 64:518–523.

681 Miriagou V, Cornaglia G, Edelstein M, Galani I, Giske CG, Gniadkowski M, Malamou-Lada
682 E, Martinez-Martinez L, Navarro F, Nordmann P, Peixe L, Pournaras S, Rossolini GM,
683 Tsakris A, Vatopoulos A, Cantón R (2010) Acquired carbapenemases in Gram-negative
684 bacterial pathogens: detection and surveillance issues. Clin Microbiol Infect 16:112–122.
685 doi: 10.1111/j.1469-0691.2009.03116.x

686 Miroshnikov KA, Faizullina NM, Sykilinda NN, Mesyanzhinov V V (2006) Properties of the
687 endolytic transglycosylase encoded by gene 144 of Pseudomonas aeruginosa
688 bacteriophage phiKZ. Biochem Biokhimiia 71:300–5. doi: 10.1134/S0006297906030102

689 Mitchell A, Chang H-Y, Daugherty L, Fraser M, Hunter S, Lopez R, McAnulla C,
690 McMenamin C, Nuka G, Pesseat S, Sangrador-Vegas A, Scheremetjew M, Rato C, Yong
691 S-Y, Bateman A, Punta M, Attwood TK, Sigrist CJA, Redaschi N, Rivoire C, Xenarios I,
692 Kahn D, Guyot D, Bork P, Letunic I, Gough J, Oates M, Haft D, Huang H, Natale DA,
693 Wu CH, Orengo C, Sillitoe I, Mi H, Thomas PD, Finn RD (2014) The InterPro protein
694 families database: the classification resource after 15 years. Nucleic Acids Res 43:D213–
695 21. doi: 10.1093/nar/gku1243

696 Morello E, Saussereau E, Maura D, Huerre M, Touqui L, Debarbieux L (2011) Pulmonary
697 bacteriophage therapy on Pseudomonas aeruginosa cystic fibrosis strains: first steps
698 towards treatment and prevention. PLoS One 6:e16963. doi:
699 10.1371/journal.pone.0016963

700 Naville M, Ghuillot-Gaudeffroy A, Marchais A, Gautheret D (2014) ARNold: A web tool for
701 the prediction of Rho-independent transcription terminators. RNA Biol 8:11–13. doi:
702 10.4161/rna.8.1.13346

703 Olszak T, Zarnowiec P, Kaca W, Danis-Wlodarczyk K, Augustyniak D, Drevinek P, de Soyza
704 A, McClean S, Drulis-Kawa Z (2015) In vitro and in vivo antibacterial activity of
705 environmental bacteriophages against Pseudomonas aeruginosa strains from cystic
706 fibrosis patients. Appl Microbiol Biotechnol. doi: 10.1007/s00253-015-6492-6

707 Pajunen M, Kiljunen S, Skurnik M (2000) Bacteriophage phiYeO3-12, specific for Yersinia
708 enterocolitica serotype O:3, is related to coliphages T3 and T7. J Bacteriol 182:5114–
709 5120. doi: 10.1128/JB.182.18.5114-5120.2000

710 Pirnay JP, De Vos D, Cochez C, Bilocq F, Vanderkelen A, Zizi M, Ghysels B, Cornelis P
711 (2002) Pseudomonas aeruginosa displays an epidemic population structure. Environ
712 Microbiol 4:898–911. doi: 10.1046/j.1462-2920.2002.00321.x

713 Poole K (2011) Pseudomonas aeruginosa: resistance to the max. Front Microbiol 2:65. doi:
714 10.3389/fmicb.2011.00065

715 Rice P, Longden I, Bleasby A (2000) EMBOSS: The European Molecular Biology Open
716 Software Suite. Trends Genet 16:276–277. doi: 10.1016/j.cocis.2008.07.002

717 Saussereau E, Vachier I, Chiron R, Godbert B, Sermet I, Dufour N, Pirnay JP, De Vos D,
718 Carrié F, Molinari N, Debarbieux L (2014) Effectiveness of bacteriophages in the
719 sputum of cystic fibrosis patients. Clin Microbiol Infect 1–8. doi: 10.1111/1469-

0691.12712

Sayers E, Barrett T, Benson D, Bolton E, Bryant S, Canese K, Chetvernin V, Church D, DiCuccio M, Federhen S, Feolo M, Fingerman I, Geer L, Helmberg W, Kapustin Y, Landsman D, Lipman D, Lu Z, Madden T, Madej T, Maglott D, Marchler-Bauer A, Miller V, Mizrachi I, Ostell J, Panchenko A, Phan L, Pruitt K, Schuler G, Sequeira E, Sherry S, Shumway M, Sirotkin K, Slotta D, Souvorov A, G S, Tatusova T, Wagner L, Wang Y, Wilbur W, Yaschenko E, Ye J (2011) Database resources of the National Center for Biotechnology Information. Nucleic Acids Res 39:D38–51. doi: doi: 10.1093/nar/gkq1172. Epub 2010 Nov 21

Schroeder TH, Reiniger N, Meluleni G, Grout M, Coleman FT, Pier GB (2001) Transgenic cystic fibrosis mice exhibit reduced early clearance of Pseudomonas aeruginosa from the respiratory tract. J Immunol 166:7410–7418. doi: 10.4049/jimmunol.166.12.7410

Söding J, Biegert A, Lupas AN (2005) The HHpred interactive server for protein homology detection and structure prediction. Nucleic Acids Res. doi: 10.1093/nar/gki408

Sokolova OS, Shaburova O V., Pechnikova E V., Shaytan AK, Krylov S V., Kiselev NA, Krylov VN (2014) Genome packaging in EL and Lin68, two giant phiKZ-like bacteriophages of P. aeruginosa. Virol 468-470C:472–478. doi: 10.1016/j.virol.2014.09.002

Sulakvelidze A, Alavidze Z, Morris Jr. JG (2001) Bacteriophage therapy minireview. Antimicrob Agents Chemother 45:649–659. doi: 10.1128/AAC.45.3.649

Thomas J a, Weintraub ST, Wu W, Winkler DC, Cheng N, Steven AC, Black LW (2012) Extensive proteolysis of head and inner body proteins by a morphogenetic protease in the giant Pseudomonas aeruginosa phage φKZ. Mol Microbiol 84:324–39. doi: 10.1111/j.1365-2958.2012.08025.x

Trautmann M, Lepper PM, Haller M (2005) Ecology of Pseudomonas aeruginosa in the intensive care unit and the evolving role of water outlets as a reservoir of the organism. Am J Infect Control 33:S41–9. doi: 10.1016/j.ajic.2005.03.006

Van den Bossche A, Ceyssens P-J, De Smet J, Hendrix H, Bellon H, Leimer N, Wagemans J, Delattre A-S, Cenens W, Aertsen A, Landuyt B, Minakhin L, Severinov K, Noben J-P, Lavigne R (2014) Systematic identification of hypothetical bacteriophage proteins targeting key protein complexes of pseudomonas aeruginosa. J Proteome Res 13:4446–56. doi: 10.1021/pr500796n

Wąsik S, Bryll A, Drabik M, Dworecki K, Ślęzak A (2015) Laser interferometric investigation of solute transport through membrane-concentration boundary layer system. J Biol Phys 41:409–420. doi: 10.1007/s10867-015-9387-y

Worlitzsch D, Tarran R, Ulrich M, Schwab U, Cekici A, Meyer KC, Birrer P, Bellon G, Berger J, Weiss T, Botzenhart K, Yankaskas JR, Randell S, Boucher RC, Döring G (2002) Effects of reduced mucus oxygen concentration in airway Pseudomonas infections of cystic fibrosis patients. J Clin Invest 109:317–325. doi: 10.1172/JCI200213870

Wright A, Hawkins CH, Anggård EE, Harper DR (2009) A controlled clinical trial of a therapeutic bacteriophage preparation in chronic otitis due to antibiotic-resistant Pseudomonas aeruginosa; a preliminary report of efficacy. Clin Otolaryngol 34:349–57. doi: 10.1111/j.1749-4486.2009.01973.x

764 Yakunina M, Artamonova T, Borukhov S, Makarova KS, Severinov K, Minakhin L (2015) A
765 non-canonical multisubunit RNA polymerase encoded by a giant bacteriophage. Nucleic
766 Acids Res gkv1095. doi: 10.1093/nar/gkv1095

767 Zabner J, Karp P, Seiler M, Phillips SL, Mitchell CJ, Saavedra M, Welsh M, Klingelhutz AJ
768 (2003) Development of cystic fibrosis and noncystic fibrosis airway cell lines. Am J
769 Physiol Lung Cell Mol Physiol 284:L844–L854. doi: 10.1152/ajplung.00355.2002

770

771

772

Tables and Figures

Table 1. Phage receptor identification on *P. aeruginosa* PAO1 mutants.

Fig 1. Protein-sharing network for KTN4. (A) A network representation was produced using the edge-weighted spring embedded layout of Cytoscape version 3.1.1. Nodes indicate phage genomes and edges between two nodes indicate their statistically weighted pairwise similarities with phage-phage similarity scores of ≥ 1. There are 495 nodes and 6,948 edges in this network; (B) An enlarged view of the circle in Panel B. Values are the similarity scores estimated with the hypergeometric equation shown in Materials and methods. Edge thickness is proportional to protein sequence identity, which is represented in the legend box.

Fig. 2. The antibacterial effect of colistin against 24 h PAO1 biofilm formed on Nephrophane membrane (A); the anti-biofilm effect of KTN4 phage/colistin treatment on 24, 48 and 72 h PAO1 biofilm formed on Nephrophane membrane: the biomass evaluation by CV staining (B); the level of pyocyanin in growth medium (C); the fluorescence of pyoverdin in growth medium (D). Untreated biofilm was used as control. The results are presented as the means ± SD. Statistical analysis was made by the ANOVA test (denoted p-values).

Fig. 3. Laser interferometry analysis of TSB medium diffusion through PAO1 biofilm treated with phages. Untreated biofilm was used as control. The results are presented as the means ± SD from three independent experiments.

Fig. 4. The 3D surface optical profile analysis of Nephrophane membrane (A); PAO1 biofilm (B); PAO1 biofilm after KTN4 phage bacteriophage degradation (C) measured by ZETA-20 instrument.

Fig. 5. Phage KTN4 treatment of *P. aeruginosa* infected NuLi-1 and CuFi -1 epithelial cells. (A) colony count of bacteria collected from apical wash; (B) colony count of bacteria internalized in epithelial cells. The results are presented as the means ± SD. Statistical analysis was made by the ANOVA test (denoted p-values).

Fig. 6. Antibacterial activity of KTN4 phage (MOI 100) in the treatment of infected *Galleria* larvae by *PA* strains. Positive control consisted of infected but untreated larvae and KTN4 control was larvae group receiving phage lysate only. Statistical analysis was calculated for pair wise comparisons between infected larvae and phage treated infected larvae using Mantel-Cox test.

Supporting information

Suppl. 1. Supplementary information of genome and proteome analysis of KTN4

Table S1. ESI-MS/MS analysis of denaturated phage particles after fractionation on SDS-PAGE gel.

Table S2. Phage activity comparison of fourteen different *Pseudomonas* phages on *P. aeruginosa* strains from Military Hospital Nederoverheembeek, Brussels, Belgium collection [Pirnay JP et al., 2002].

Table S3. The Nephrophane roughness (R) parameters measured by ZETA-20.

Fig. S1. Transmission electron microscopic images of phage KTN4. The scale bar represents 100nm.

Fig S2. Alignments of KTN4 promoters. (A) Early promoters. The 5’ ends of primer extension products, which correspond to the transcription start sites, are located ~ 10 bp downstream from the center of the core TATATTAC motif and are associated with an additional conserved 5’-TG-3'motif. (B) Middle promoters. They are united by only a weak AT-rich motif (5’-AAanntTAC-3’; lowercase letters represent a lower level of conservation) centered at position 24 with respect to the transcription start site (C) Late promoters. No sequence conservation upstream of 5’ ends of late transcripts could be detected apart from a 5’-TATG-3’ motif overlapping the transcription start site. The corresponding sequence logos are depicted below the alignments. Pink bars delineate conserved promoter elements.

Fig S3. Phage KTN4 predicted terminators with palindromes marked blue.

Fig. S4. SDS-PAGE pattern of KTN4 structural proteome against Page Ruler Prestained Protein Ladder (Thermo Scientific) in first line. The corresponding molecular weight is mentioned left. The numbered fractions on the right, correspond to gel slices analyzed individually by ESI-MS/MS. The proteins are mentioned in the slice in which they were most abundantly present.

Tables and Figures

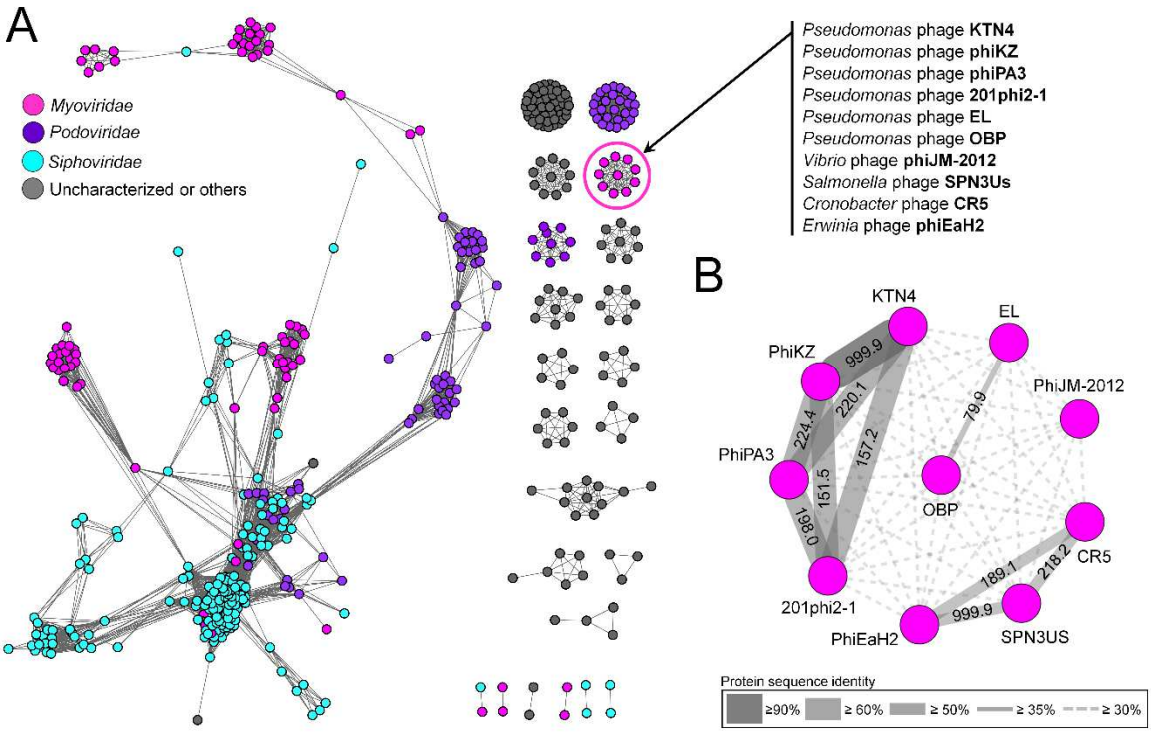

Fig 1. Protein-sharing network for KTN4. (A) A network representation was produced using the edge-weighted spring embedded layout of Cytoscape version 3.1.1. Nodes indicate phage genomes and edges between two nodes indicate their statistically weighted pairwise similarities with phage-phage similarity scores of ≥ 1. There are 495 nodes and 6,948 edges in this network; (B) An enlarged view of the circle in Panel B. Values are the similarity scores estimated with the hypergeometric equation shown in Materials and methods. Edge thickness is proportional to protein sequence identity, which is represented in the legend box.

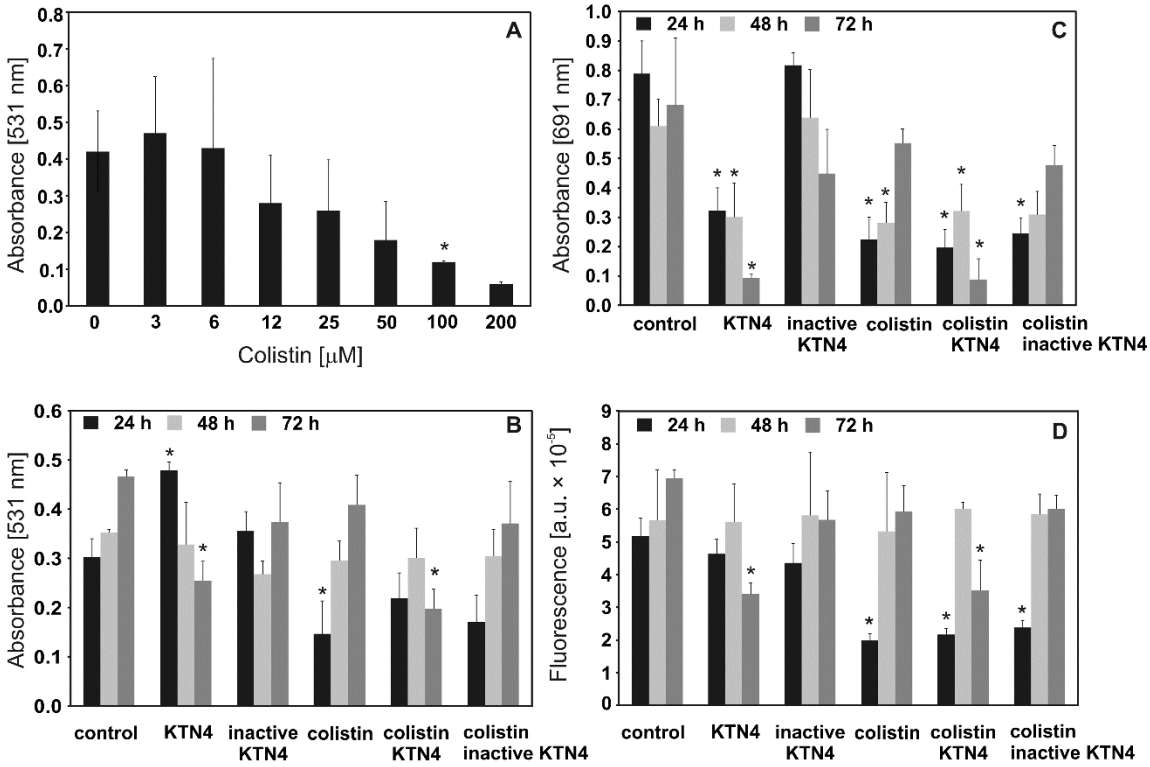

839

840 **Fig. 2.** The antibacterial effect of colistin against 24 h PA01 biofilm formed on Nephrophane
841 membrane (A); the anti-biofilm effect of KTN4 phage/colistin treatment on 24, 48 and 72 h
842 PA01 biofilm formed on Nephrophane membrane: the biomass evaluation by CV staining (B);
843 the level of pyocyanin in growth medium (C); the fluorescence of pyoverdin in growth medium
844 (D). Untreated biofilm was used as control. The results are presented as the means ± SD.
845 Statistical analysis was made by the ANOVA test (denoted p-values).

846

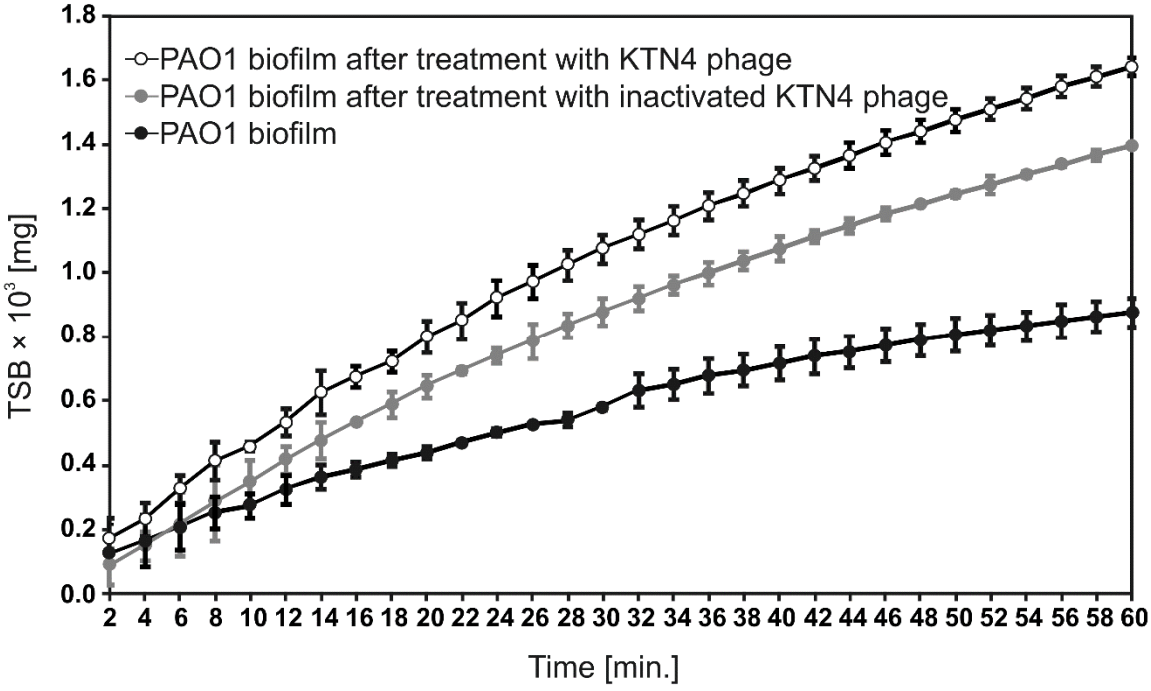

847

848 **Fig. 3.** Laser interferometry analysis of TSB medium diffusion through PA01 biofilm treated
849 with phages. Untreated biofilm was used as control. The results are presented as the means ±
850 SD from three independent experiments.

851

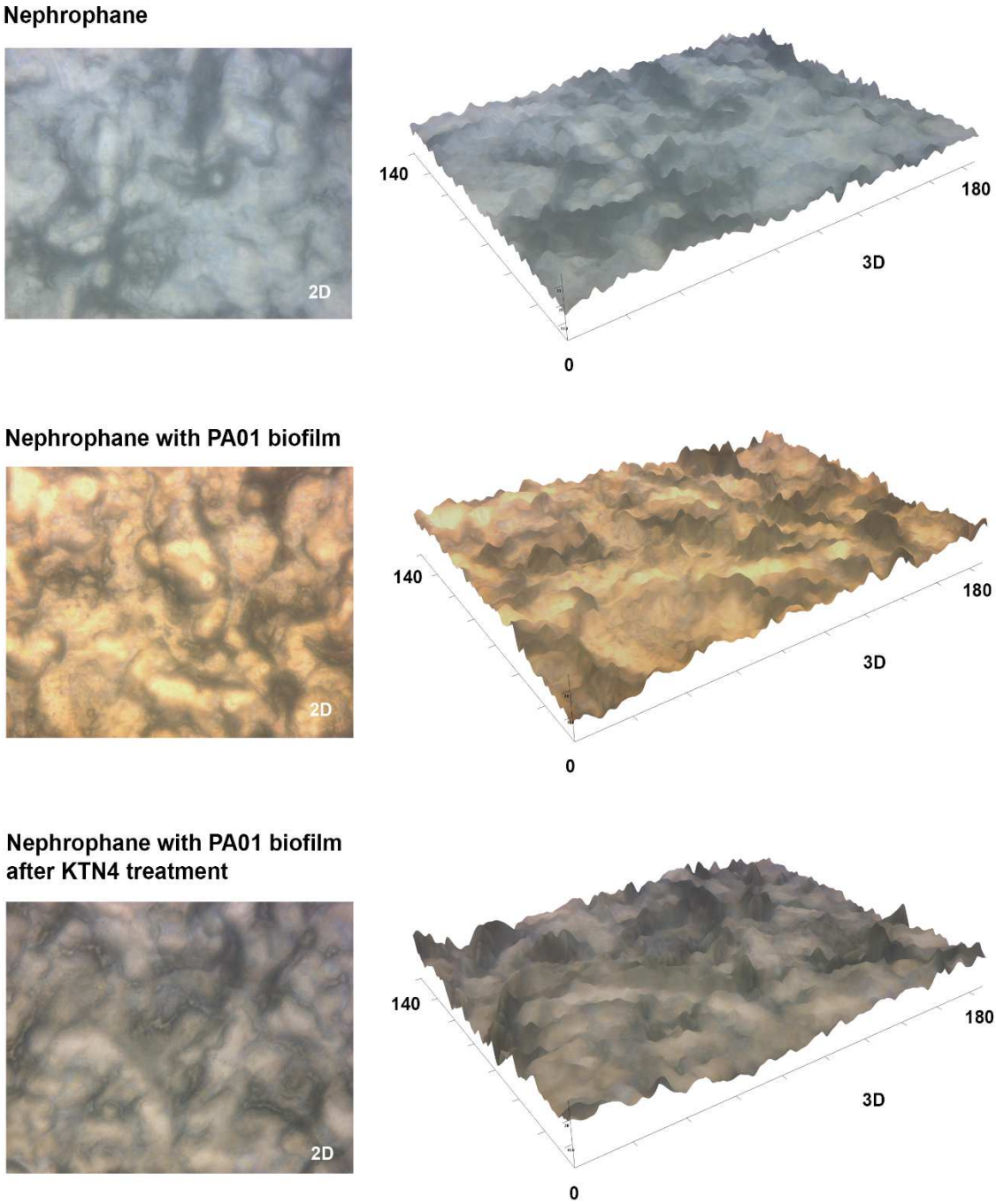

852

853 **Fig. 4.** The 3D surface optical profile analysis of Nephrophane membrane (A); PA01 biofilm

854 (B); PA01 biofilm after KTN4 phage bacteriophage degradation (C) measured by ZET 20

855 instrument.

856

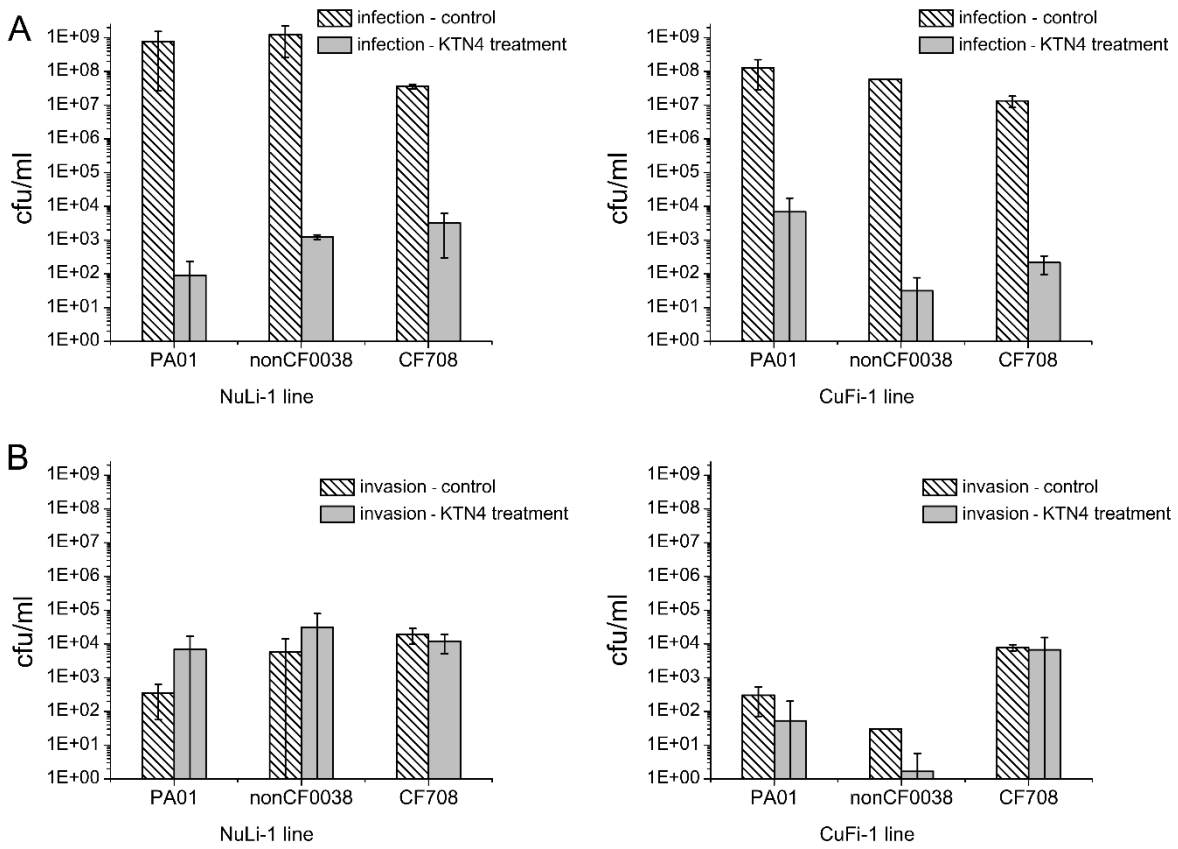

857

858 **Fig. 5.** Phage KTN4 treatment of *P. aeruginosa* infected NuLi-1 and CuFi -1 epithelial cells.
859 (A) colony count of bacteria collected from apical wash; (B) colony count of bacteria
860 internalized in epithelial cells. The results are presented as the means ± SD. Statistical analysis
861 was made by the ANOVA test (denoted p-values).

862

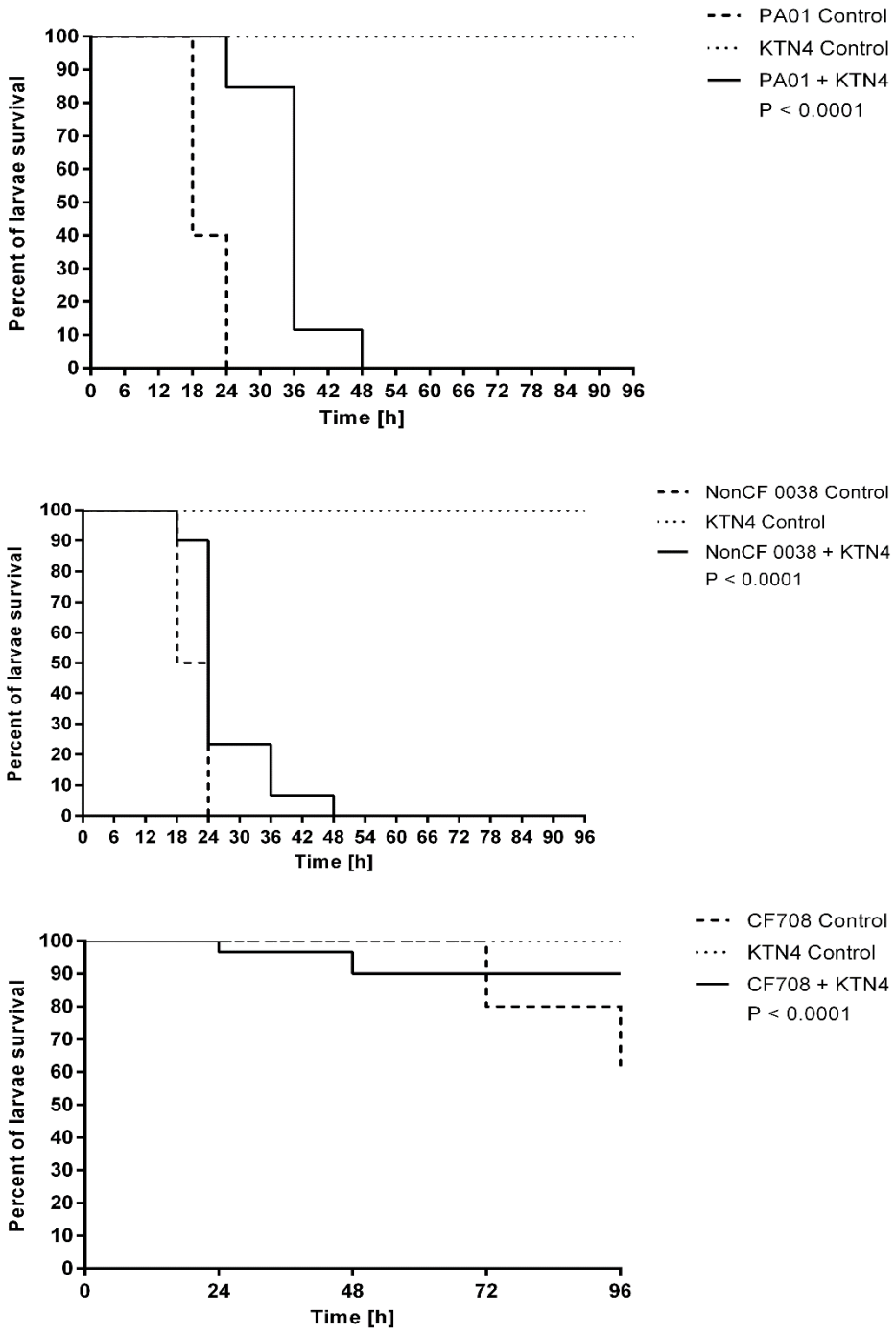

Fig. 6. Antibacterial activity of KTN4 phage (MOI 100) in the treatment of infected *Galleria* larvae by *PA* strains. Positive control consisted of infected but untreated larvae and KTN4 control was larvae group receiving phage lysate only. Statistical analysis was calculated for pair wise comparisons between infected larvae and phage treated infected larvae using Mantel-Cox test.

869 **Table 1.** Phage receptor identification on *P. aeruginosa* PA01 mutants.

Bacterial strain	**Phenotype**	**Origin**	**KTN4**	**φKZ**
PAO1 (ATCC 15692)	Wild type	American Type Culture Collection	+	+
PAO1 Pirnay	Wild type with inactive type IV pili	Military Hospital Nederoverheembeek, Brussels, Belgium, Dr. Jean-Paul Pirnay	-	-
PAO1 Krylov	Wild type	Military Hospital Nederoverheembeek, Brussels, Belgium, Dr. Jean-Paul Pirnay	+	+
PAO1 Δrmd (A-, B+)	Deficiency in D-rhamnose biosynthesis; lack of A-band LPS	Laboratory of Foodborne Zoonoses, Guelph, Canada, Andrew M. Kropinski	+	+
PAO1 ΔrmLC (A-, B-, core-)	Deficiency in L-rhamnose biosynthesis; truncate core region, lack of A-band and B-band LPS	Laboratory of Foodborne Zoonoses, Guelph, Canada, Andrew M. Kropinski	+	+
PAO1 ΔwaaL (A-, B-)	Lack of WaaL ligating O-polymer to core-lipid A; LPS is devoid of A-band and B-band, semirough (SR-LPS, or core-plus-one O-antigen)	Laboratory of Foodborne Zoonoses, Guelph, Canada, Andrew M. Kropinski	+	+
PAO1 ΔwbpL (A-, B-)	Lack of glucosyltransferase WbpL essential for initiation of both A-band and B-band synthesis	Laboratory of Foodborne Zoonoses, Guelph, Canada, Andrew M. Kropinski	+	+

PAO1 ΔfliC ΔalgC ΔpilA	Lack of flagella; lack of AlgC required for A-band, core oligosaccharide, and alginate biosynthesis; lack of type IV pili	Technical University Hamburg, Germany, Max Schöbert	-	-
PAO1 ΔfliC wt algC ΔpilA	Lack of flagella; lack of type IV pili	Technical University Hamburg, Germany, Max Schöbert	-	-
PAO1 ΔfliC wt algC wt pilA	Lack of flagella	Technical University Hamburg, Germany, Max Schöbert	+	+
PAO1 wt fliC wt algC wt pilA	Wild type	Technical University Hamburg, Germany, Max Schöbert	+	+

870

871
872

Supporting information

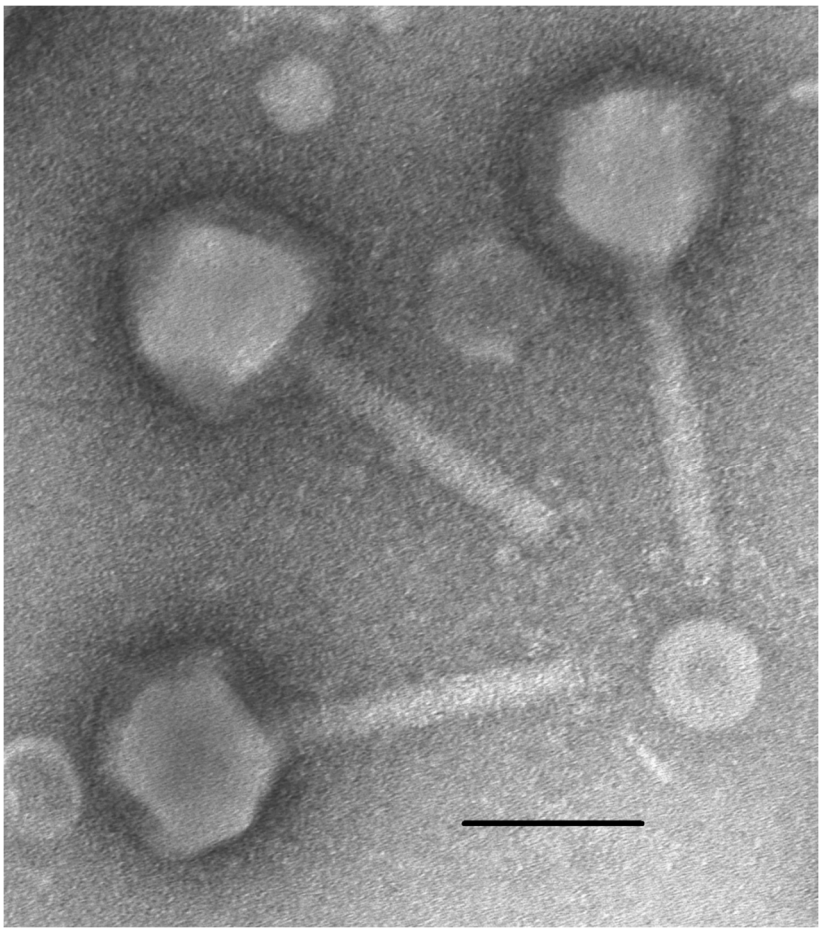

Fig. S1. Transmission electron microscopic images of phage KTN4. The scale bar represents 100nm.

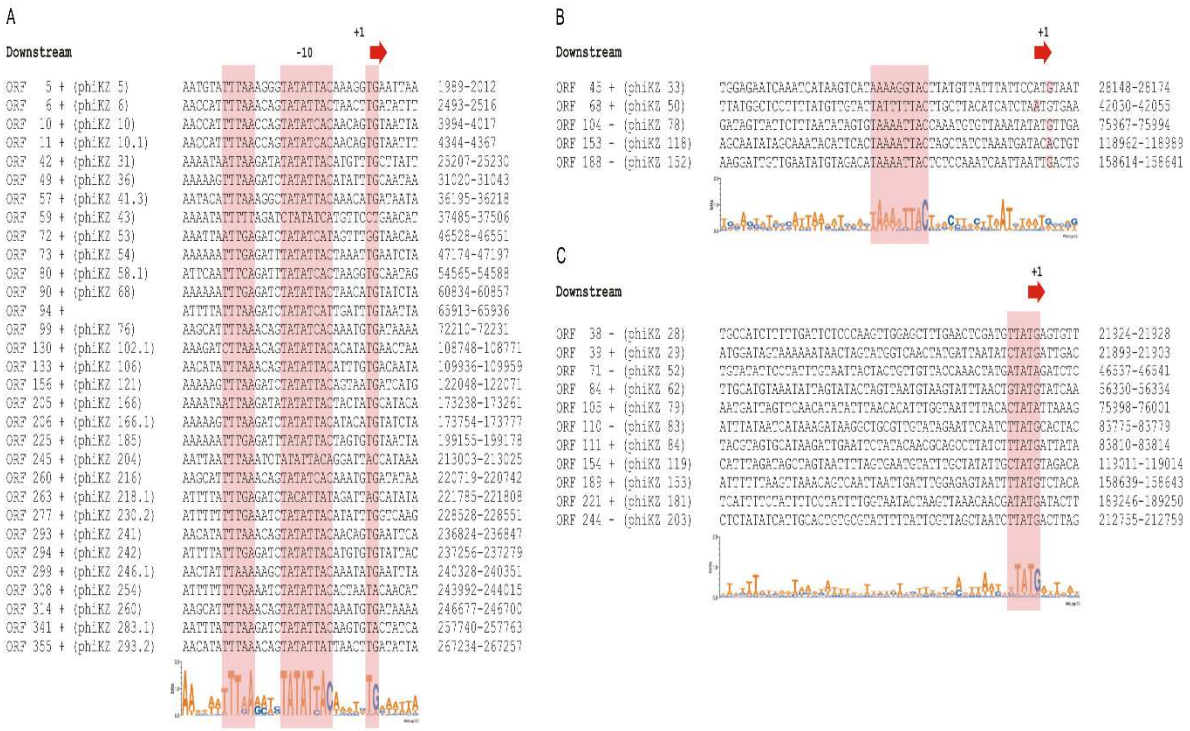

878

879 **Fig S2.** Alignments of KTN4 promoters. (A) Early promoters. The 5’ ends of primer extension
880 products, which correspond to the transcription start sites, are located ~ 10 bp downstream from
881 the center of the core TATATTAC motif and are associated with an additional conserved 5’-
882 TG-3'motif. (B) Middle promoters. They are united by only a weak AT-rich motif (5’-
883 AAanntTAC-3’; lowercase letters represent a lower level of conservation) centered at position
884 24 with respect to the transcription start site (C) Late promoters. No sequence conservation
885 upstream of 5’ ends of late transcripts could be detected apart from a 5’-TATG-3’ motif
886 overlapping the transcription start site. The corresponding sequence logos are depicted below
887 the alignments. Pink bars delineate conserved promoter elements.

888

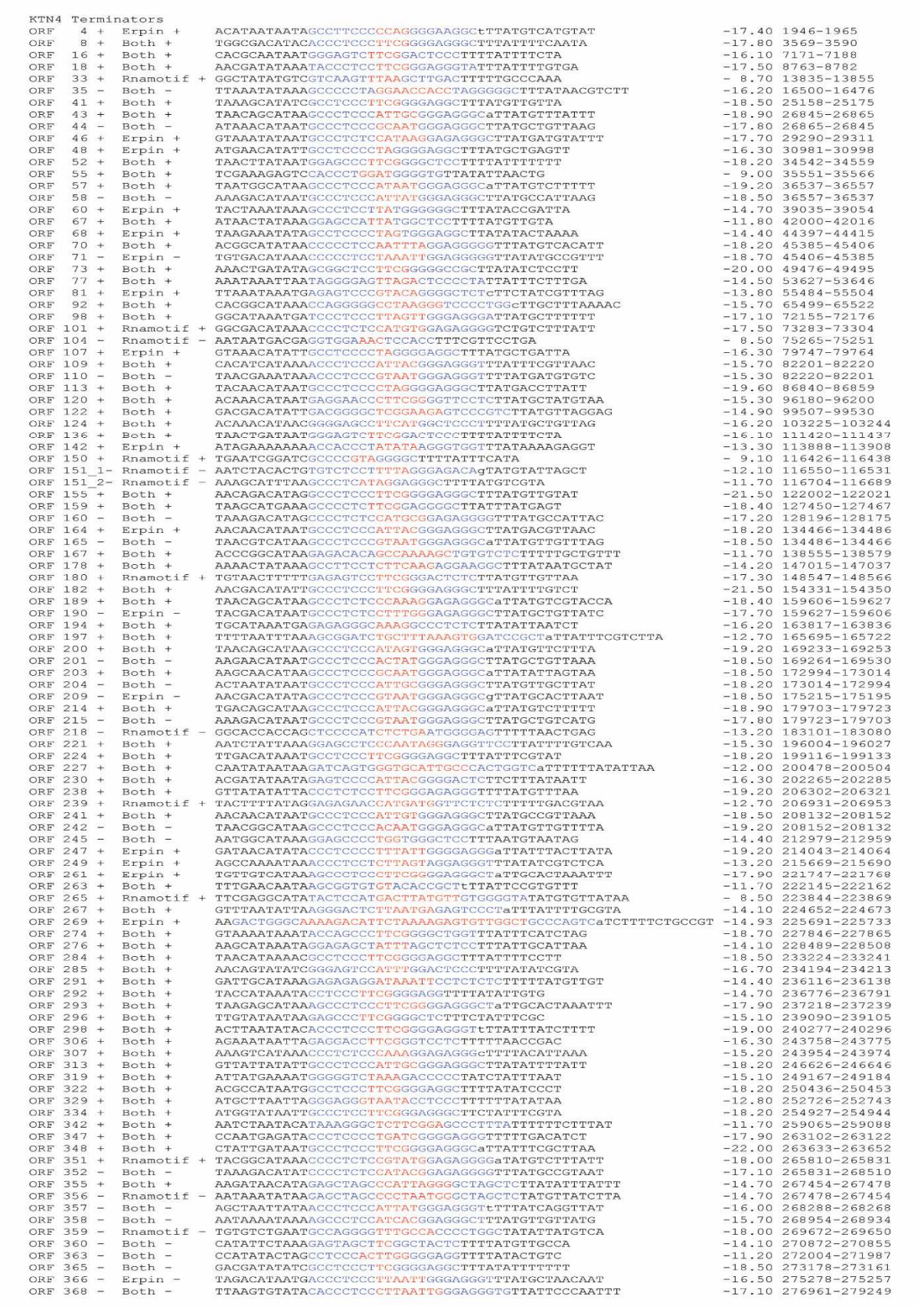

KTN4 Terminators

ORF	4	+	Erpin	+	ACATAATAATAGCCTTCCCCCAGGGGAAGGCtTTATGTCATGTAT	-17.40 1946-1965
ORF	8	+	Both	+	TGGCGACATACACCCTCCCTTCGGGGAGGGCTTTATTTTCAATA	-17.80 3569-3590
ORF	16	+	Both	+	CACGCAATAATGGGAGTCTTCGGACTCCCTTTTATTTTCTA	-16.10 7171-7188
ORF	18	+	Both	+	AACGATATAAATACCCTCCTTCGGGAGGGTATTTATTTTGTGA	-17.50 8763-8782
ORF	33	+	Rnamotif	+	GGCTATATGTCGTCAAGTTTAAGCTTGACTTTTTGCCCAAA	- 8.70 13835-13855
ORF	35	-	Both	-	TTAAATATAAAGCCCCCTAGGAACCACCTAGGGGGCTTTATAACGTCTT	-16.20 16500-16476
ORF	41	+	Both	+	TAAAGCATATCGCCTCCCTTCGGGGAGGCTTTATGTTGTTA	-18.50 25158-25175
ORF	43	+	Both	+	TAACAGCATAAGCCCTCCCATTGCGGGAGGGCaTTATGTTTATTT	-18.90 26845-26865
ORF	44	-	Both	-	ATAAACATAATGCCCTCCCGCAATGGGAGGGCTTATGCTGTTAAG	-17.80 26865-26845
ORF	46	+	Erpin	+	GTAAATATAATGCCCTCTCCATAAGGAGAGGGCTTATGATGTATTT	-17.70 29290-29311
ORF	48	+	Erpin	+	ATGAACATATTGCCTCCCCTAGGGGAGGCTTTATGCTGAGTT	-16.30 30981-30998
ORF	52	+	Both	+	TAACTTATAATGGAGCCCTTCGGGGCTCCTTTTATTTTTTT	-18.20 34542-34559
ORF	55	+	Both	+	TCGAAAGAGTCCACCCTGGATGGGGTGTTATATTAACTG	- 9.00 35551-35566
ORF	57	+	Both	+	TAATGGCATAAGCCCTCCCATAATGGGAGGGCaTTATGTCTTTTT	-19.20 36537-36557
ORF	58	-	Both	-	AAAGACATAATGCCCTCCCATTATGGGAGGGCTTATGCCATTAAG	-18.50 36557-36537
ORF	60	+	Erpin	+	TACTAAATAAAGCCCTCCTTATGGGGGGCTTTATACCGATTA	-14.70 39035-39054
ORF	67	+	Both	+	ATAACTATAAAGGAGCCATTATGGCTCCTTTTATGTTGTA	-11.80 42000-42016
ORF	68	+	Erpin	+	TAAGAAATATAGCCTCCCCTAGTGGGAGGCTTATATACTAAAA	-14.40 44397-44415
ORF	70	+	Both	+	ACGGCATATAACCCCCTCCAATTTAGGAGGGGGTTTATGTCACATT	-18.20 45385-45406
ORF	71	-	Erpin	-	TGTGACATAAACCCCCTCCTAAATTGGAGGGGGTTATATGCCGTTT	-18.70 45406-45385
ORF	73	+	Both	+	AAACTGATATAGCGGCTCCTTCGGGGGCCGCTTATATCTCCTT	-20.00 49476-49495
ORF	77	+	Both	+	AAATAAATTAATAGGGGAGTTAGACTCCCCTATTATTTCTTTGA	-14.50 53627-53646
ORF	81	+	Erpin	+	TTAAATAAATGAGAGTCCCGTACAGGGGCTCTcTTCTATCGTTTAG	-13.80 55484-55504
ORF	92	+	Both	+	CACGGCATAAACCAGGGGGCCTAAGGGTCCCCTGGcTTGCTTTAAAAC	-15.70 65499-65522
ORF	98	+	Both	+	GGCATAAATGATCCCTCCCTTAGTTGGGAGGGATTATGCTTTTTT	-17.10 72155-72176
ORF	101	+	Rnamotif	+	GGCGACATAAACCCCTCTCCATGTGGAGAGGGGTCTGTCTTTATT	-17.50 73283-73304
ORF	104	-	Rnamotif	-	AATAATGACGAGGTGGAAACTCCACCTTTCGTTCCTGA	- 8.50 75265-75251
ORF	107	+	Erpin	+	GTAAACATATTGCCTCCCCTAGGGGAGGCTTTATGCTGATTA	-16.30 79747-79764
ORF	109	+	Both	+	CACATCATAAAACCCTCCCATTACGGGAGGGTTTATTTCGTTAAC	-15.70 82201-82220
ORF	110	-	Both	-	TAACGAAATAAACCCTCCCGTAATGGGAGGGTTTTATGATGTGTC	-15.30 82220-82201
ORF	113	+	Both	+	TACAACATAATGCCCTCCCCTAGGGGAGGGCTTATGACCTTATT	-19.60 86840-86859
ORF	120	+	Both	+	ACAAACATAATGAGGAACCCTTCGGGGGTTCCTCTTATGCTATGTAA	-15.30 96180-96200
ORF	122	+	Both	+	GACGACATATTGACGGGGCTCGGAAGAGTCCCGTCTTATGTTAGGAG	-14.90 99507-99530
ORF	124	+	Both	+	ACAAACATAACGGGGAGCCTTCATGGCTCCCTTTTATGCTGTTAG	-16.20 103225-103244
ORF	136	+	Both	+	TAACTGATAATGGGAGTCTTCGGACTCCCTTTTATTTTCTA	-16.10 111420-111437
ORF	142	+	Erpin	+	ATAGAAAAAAAACCACCCTATATAAGGGTGGTTTATAAAAGAGGT	-13.30 113888-113908
ORF	150	+	Rnamotif	+	TGAATCGGATCGCCCCGTAGGGGCTTTTATTTCATA	- 9.10 116426-116438
ORF	151_1	-	Rnamotif	-	AATCTACACTGTGTCTCCTTTTAGGGAGACAgTATGTATTAGCT	-12.10 116550-116531
ORF	151_2	-	Rnamotif	-	AAAGCATTTAAGCCCTCATAGGAGGGCTTTTATGTCGTA	-11.70 116704-116689
ORF	155	+	Both	+	AACAGACATAGGCCCTCCCTTCGGGGAGGGCTTTATGTTGTAT	-21.50 122002-122021
ORF	159	+	Both	+	TAAGCATGAAAGCCCCTCTTCGGAGGGGCTTATTTATGAGT	-18.40 127450-127467
ORF	160	-	Both	-	TAAAGACATAGCCCCTCTCCATGCGGAGAGGGGTTTATGCCATTAC	-17.20 128196-128175
ORF	164	+	Erpin	+	AACAACATAATGCCCTCCCATTACGGGAGGGCTTATGACGTTAAC	-18.20 134466-134486
ORF	165	-	Both	-	TAACGTCATAAGCCCTCCCGTAATGGGAGGGCaTTATGTTGTTTAG	-18.50 134486-134466
ORF	167	+	Both	+	ACCCGGCATAAGAGACACAGCCAAAAGCTGTGTCTCTTTTTGCTGTTT	-11.70 138555-138579
ORF	178	+	Both	+	AAAACTATAAAGCCTTCCTCTTCAAGAGGAAGGCTTTATAATGCTAT	-14.20 147015-147037
ORF	180	+	Rnamotif	+	TGTAACTTTTTGAGAGTCCTTCGGGACTCTCTTATGTTGTTAA	-17.30 148547-148566
ORF	182	+	Both	+	AACGACATATTGCCCTCCCTTCGGGGAGGGCTTTATTTTGTCT	-21.50 154331-154350
ORF	189	+	Both	+	TAACAGCATAAGCCCTCTCCCAAAGGAGAGGGCaTTATGTCGTACCA	-18.40 159606-159627
ORF	190	-	Erpin	-	TACGACATAATGCCCTCTCCTTTGGGAGAGGGCTTATGCTGTTATC	-17.70 159627-159606
ORF	194	+	Both	+	TGCATAAATGAGAGAGGGCAAAGGCCCTCTCTTATATTAATCT	-16.20 163817-163836
ORF	197	+	Both	+	TTTTAATTTAAAGCGGATCTGCTTTAAAGTGGATCCGCTaTTATTTCGTCTTA	-12.70 165695-165722
ORF	200	+	Both	+	TAACAGCATAAGCCCTCCCATAGTGGGAGGGCaTTATGTTCTTTA	-19.20 169233-169253
ORF	201	-	Both	-	AAGAACATAATGCCCTCCCACTATGGGAGGGCTTATGCTGTTAAA	-18.50 169264-169530
ORF	203	+	Both	+	AAGCAACATAAGCCCTCCCGCAATGGGAGGGCaTTATATTAGTAA	-18.50 172994-173014
ORF	204	-	Both	-	ACTAATATAATGCCCTCCCATTGCGGGAGGGCTTATGTTGCTTAT	-18.20 173014-172994
ORF	209	-	Erpin	-	AACGACATATAGCCCTCCCGTAATGGGAGGGCgTTATGCACTTAAT	-18.50 175215-175195
ORF	214	+	Both	+	TGACAGCATAAGCCCTCCCATTACGGGAGGGCaTTATGTCTTTTT	-18.90 179703-179723
ORF	215	-	Both	-	AAAGACATAATGCCCTCCCGTAATGGGAGGGCTTATGCTGTCATG	-17.80 179723-179703
ORF	218	-	Rnamotif	-	GGCACCACCAGGCTCCCCATCTCTGAATGGGGAGTTTTTAACTGAG	-13.20 183101-183080
ORF	221	+	Both	+	AATCTATTAAAGGAGCCTCCCAATAGGGAGGTTCCTTATTTTGTCAA	-15.30 196004-196027
ORF	224	+	Both	+	TTGACATAAATGCCTCCCTTCGGGGAGGCTTTATTTCGTAT	-18.20 199116-199133
ORF	227	+	Both	+	CAATATAATAAGATCAGTGGGTGCATTGCCCACTGGTCaTTTTTTATATTAA	-12.00 200478-200504
ORF	230	+	Both	+	ACGATATAATAGAGTCCCCATTACGGGGACTCTTCTTTATAATT	-16.30 202265-202285
ORF	238	+	Both	+	GTTATATATTACCCTCTCCTTCGGGAGAGGGTTTTATGTTTAA	-19.20 206302-206321
ORF	239	+	Rnamotif	+	TACTTTTATAGGAGAGAACCATGATGGTTCTCTCTTTTTGACGTAA	-12.70 206931-206953
ORF	241	+	Both	+	AACAACATAATGCCCTCCCATTGTGGGAGGGCTTATGCCGTTAAA	-18.50 208132-208152
ORF	242	-	Both	-	TAACGGCATAAGCCCTCCCACAATGGGAGGGCaTTATGTTGTTTTA	-19.20 208152-208132
ORF	245	-	Both	-	AATGGCATAAAGGAGCCCCTGGTGGGCTCCTTTAATGTAATAG	-14.40 212979-212959
ORF	247	+	Erpin	+	GATAACATATACCCTCCCCTTTATTGGGGAGGGaTTATTTACTTATA	-19.20 214043-214064
ORF	249	+	Erpin	+	AGCCAAAATAAACCCTCCTCTTAGTAGGAGGGTTTATATCGTCTCA	-13.20 215669-215690
ORF	261	+	Erpin	+	TGTTGTCATAAAGCCCTCCCTTCGGGGAGGGCTaTTGCACTAAATTT	-17.90 221747-221768
ORF	263	+	Both	+	TTTGAACAATAAGCGGTGTGTACACCGCTtTTATTCCGTGTTT	-11.70 222145-222162
ORF	265	+	Rnamotif	+	TTCGAGGCATATACTCCATGACTTATGTTGTGGGGTATATGTGTTATAA	- 8.50 223844-223869
ORF	267	+	Both	+	GTTTAATATTAAGGGACTCTTAATGAGAGTCCCTaTTTATTTTGCGTA	-14.10 224652-224673
ORF	269	+	Erpin	+	AAGACTGGGCAAAAGACATTCTAAAAGAGTGTTGGCTGCCCAGTCaTCTTTTCTGCCGT	-14.93 225691-225733
ORF	274	+	Both	+	GTAAAATAAATACCAGCCCTTCGGGGCTGGTTTATTTCATCTAG	-18.70 227846-227865
ORF	276	+	Both	+	AAGCATAAATAGGAGAGCTATTTAGCTCTCCTTTATTGCATTAA	-14.10 228489-228508
ORF	284	+	Both	+	TAACATAAAACGCCTCCCTTCGGGGAGGCTTTATTTTCCTT	-18.50 233224-233241
ORF	285	+	Both	+	AACAGTATATCGGGAGTCCATTTGGACTCCCTTTTATATCGTA	-16.70 234194-234213
ORF	291	+	Both	+	GATTGCATAAAGAGAGAGGATAAATTCCTCTCTCTTTTTATGTTGT	-14.40 236116-236138
ORF	292	+	Both	+	TACCATAAATACCTCCCTTCGGGGAGGTTTTATATTGTG	-14.70 236776-236791
ORF	293	+	Both	+	TAAGAGCATAAAGCCCTCCCTTCGGGGAGGGCTaTTGCACTAAATTT	-17.90 237218-237239
ORF	296	+	Both	+	TTGTATAATAAGAGCCCTTCGGGGCTCTTTCTATTTCGC	-15.10 239090-239105
ORF	298	+	Both	+	ACTTAATATACACCCTCCCTTCGGGGAGGGTtTTATTTATCTTTT	-19.00 240277-240296
ORF	306	+	Both	+	AGAAATAATTAGAGGACCTTCGGGTCCTCTTTTTAACCGAC	-16.30 243758-243775
ORF	307	+	Both	+	AAAGTCATAAACCCTCTCCCAAAGGAGAGGGcTTTTACATTAAA	-15.20 243954-243974
ORF	313	+	Both	+	GTTATTATATTGCCCTCCCATTGCGGGAGGGCTTATATTTTATT	-18.20 246626-246646
ORF	319	+	Both	+	ATTATGAAAATGGGGGTCTAAAGACCCCCTATCTATTTAAT	-15.10 249167-249184
ORF	322	+	Both	+	ACGCCATAATGGCCTCCCTTCGGGGAGGCTTTTATATCCCT	-18.20 250436-250453
ORF	329	+	Both	+	ATGCTTAATTAGGGAGGGTAATACCTCCCTTTTTTATATAA	-12.80 252726-252743
ORF	334	+	Both	+	ATGGTATAATTGCCCTCCTTCGGGAGGGCTTCTATTTCGTA	-18.20 254927-254944
ORF	342	+	Both	+	AATCTAATACATAAAGGGCTCTTCGGAGCCCTTTATTTTTCTTTAT	-11.70 259065-259088
ORF	347	+	Both	+	CCAATGAGATACCCTCCCCTGATCGGGGAGGGTTTTTGACATCT	-17.90 263102-263122
ORF	348	+	Both	+	CTATTGATAATGCCCTCCCTTCGGGGAGGGCaTTATTTCGCTTAA	-22.00 263633-263652
ORF	351	+	Rnamotif	+	TACGGCATAAACCCCTCTCCGTATGGAGAGGGGaTATGTCTTTATT	-18.00 265810-265831
ORF	352	-	Both	-	TAAAGACATATCCCCTCTCCATACGGAGAGGGGTTTATGCCGTAAT	-17.10 265831-265810
ORF	355	+	Both	+	AAGATAACATAGAGCTAGCCATTAGGGGCTAGCTCTTATATTTATTT	-14.70 267454-267478
ORF	356	-	Rnamotif	-	AATAAATATAAGAGCTAGCCCCTAATGGGCTAGCTCTATGTTATCTTA	-14.70 267478-267454
ORF	357	-	Both	-	AGCTAATTATAACCCTCCCATTATGGGAGGGTtTTTATCAGGTTAT	-16.00 268288-268268
ORF	358	-	Both	-	AATAAAATAAAAGCCCTCCATCACGGAGGGCTTTATGTTGTTATG	-15.70 268954-268934
ORF	359	-	Rnamotif	-	TGTGTCTGAATGCCAGGGGTTTGCCACCCCTGGCTATATTATGTCA	-18.00 269672-269650
ORF	360	-	Both	-	CATATTCTAAAGAGTAGCTTCGGCTACTCTTTTATGTTGCCA	-14.10 270872-270855
ORF	363	-	Both	-	CCATATACTAGCCTCCCACTTGGGGGAGGTTTTATACTGTC	-11.20 272004-271987
ORF	365	-	Both	-	GACGATATATCGCCTCCCTTCGGGGAGGCTTTATATTTTTTT	-18.50 273178-273161
ORF	366	-	Erpin	-	TAGACATAATGACCCTCCCTTAATTGGGAGGGTTTATGCTAACAAT	-16.50 275278-275257
ORF	368	-	Both	-	TTAAGTGTATACACCCTCCCTTAATTGGGAGGGTGTTATTCCCAATTT	-17.10 276961-279249

Fig S3. Phage KTN4 predicted terminators with palindromes marked blue.

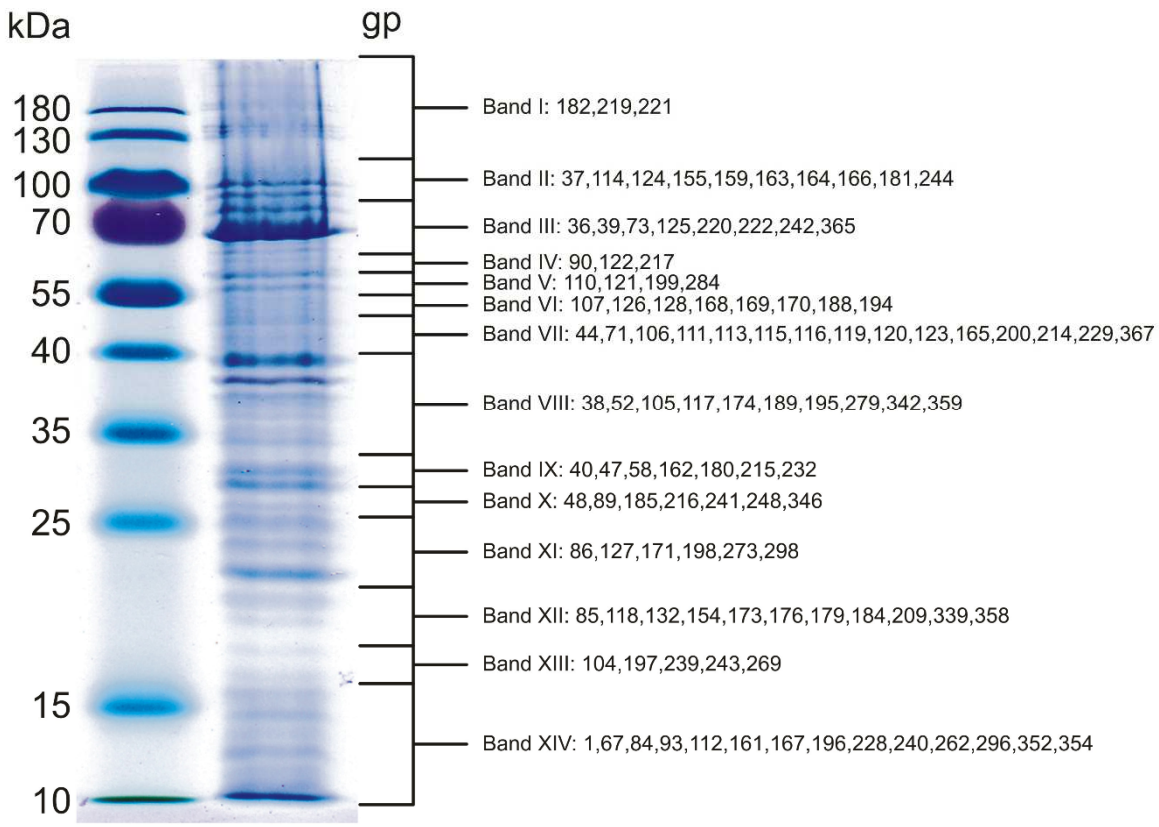

Fig. S4. SDS-PAGE pattern of KTN4 structural proteome against Page Ruler Prestained Protein Ladder (Thermo Scientific) in first line. The corresponding molecular weight is mentioned left. The numbered fractions on the right, correspond to gel slices analyzed individually by ESI-MS/MS. The proteins are mentioned in the slice in which they were most abundantly present.

898

899 **Table S1.** ESI-MS/MS analysis of denaturated phage particles after fractionation on SDS-
900 PAGE gel.

№	Protein	Identified function	Band №	Molecular weight (DA)		Number of identified peptides	Sequence coverage	Identity with other phages (BLASTP)			
				MS	SDS-PAGE			phiKZ	PhiPAK3	201phi2-1	PA7
1	gp1	Uncharacterized protein	14	14673.80	14563.8	3	35.66%	99%	37%	39%	-
2	gp36	Structural head protein	3	62440.10	62330.1	26	81.50%	99%	58%	54%	99%
3	gp37	Structural head protein	2	106511.10	106401.1	32	55.70%	99%	57%	48%	-
4	gp38	Structural head protein	8	36785.70	36675.7	13	63.44%	100%	49%	44%	99%
5	gp39	Tail sheath protein	3	79511.20	79401.2	33	78.78%	99%	69%	63%	98%
6	gp40	Structural protein	9	32658.70	32548.7	14	73.47%	100%	73%	76%	-
7	gp44	Structural head protein	7	50478.80	50368.8	19	60.20%	98%	64%	54%	98%
8	gp47	Structural protein	9	30253.60	30143.6	9	50.00%	99%	45%	40%	-
9	gp48	Structural head protein	10	29956.50	29846.5	7	80.30%	98%	-	-	-
10	gp52	Chain A monomeric subunit of Tubz	8	36567.20	36457.2	2	12.65%	99%	37%	31%	-
11	gp58	Uncharacterized protein	9	30615.90	30505.9	6	32.44%	99%	71%	61%	-
12	gp67	Uncharacterized protein	14	15500.60	15390.6	3	36.03%	98%	46%	44%	98%
13	gp71	Structural head protein	7	43687.90	43577.9	13	51.92%	100%	55%	52%	99%
14	gp73	Uncharacterized protein	3	70889.30	70779.3	14	33.01%	98%	48%	41%	98%
15	gp84	Uncharacterized protein	14	16424.50	16314.5	6	71.32%	99%	37%	31%	-
16	gp85	Uncharacterized protein	12	20854.40	20744.4	7	55.68%	95%	-	-	95%
17	gp86	Uncharacterized protein	11	24057.30	23947.3	3	21.14%	96%	39%	32%	96%
18	gp89	Uncharacterized protein	10	28962.10	28852.1	9	47.56%	100%	55%	53%	-
19	gp90	Non-virion DNA-dependent RNA polymerase subunit*	5	60527.30	60417.3	2	7.90%	99%	58%	50%	99%
20	gp93	Uncharacterized protein	14	14936.80	14826.8	5	70.83%	-	-	36%	100%
21	gp104	Uncharacterized protein	13	19031.70	18921.7	4	33.13%	96%	-	26%	98%
22	gp105	Structural head protein	8	34798.90	34688.9	12	63.60%	99%	47%	38%	99%
23	gp106	β/β′-like virion-associated proteins	7	50834.20	50724.2	16	55.95%	99%	65%	56%	99%

24	gp107	Structural protein	6	54795.30	54685.3	23	80.47%	99%	37%	31%	99%
25	gp110	Structural head protein	5	56385.00	56275	12	42.68%	97%	85%	-	98%
26	gp111	Structural head protein	7	47327.00	47217	19	64.16%	100%	37%	34%	-
27	gp112	Structural head protein	14	17092.70	16982.7	7	83.89%	99%	35%	33%	-
28	gp113	Structural head protein	7	49280.00	49170	15	43.06%	99%	25%	26%	99%
29	gp114	Structural protein	2	110487.40	110377.4	30	50.57%	99%	58%	52%	99%
30	gp115	Structural protein	7	40628.10	40518.1	7	28.53%	99%	58%	56%	-
31	gp116	Structural head protein	7	44414.80	44304.8	14	51.71%	98%	63%	54%	-
32	gp117	Structural head protein	8	36014.60	35904.6	19	78.96%	100%	49%	47%	-
33	gp118	Structural head protein	12	21586.50	21476.5	6	52.27%	99%	53%	51%	-
34	gp119	Structural head protein	7	50842.60	50732.6	17	50.00%	99%	38%	35%	99%
35	gp120	Structural head protein	7	48412.40	48302.4	16	44.03%	98%	26%	-	98%
36	gp121	Structural head protein	6	56940.00	56830	16	51.51%	98%	27%	30%	97%
37	gp122	Structural head protein	4	59192.20	59082.2	26	64.11%	98%	-	-	97%
38	gp123	Structural head protein	7	42552.20	42442.2	11	35.70%	99%	34%	28%	-
39	gp124	Structural head protein	2	89012.60	88902.6	20	39.43%	97%	31%	29%	99%
40	gp125	Uncharacterized protein	3	63780.40	63670.4	6	13.76%	99%	48%	42%	-
41	gp126	Structural head protein	4	55292.40	55182.4	12	37.53%	99%	59%	54%	-
42	gp127	Uncharacterized protein	11	22993.10	22883.1	3	25.93%	97%	47%	36%	-
43	gp128	Structural protein	4	52562.30	52452.3	7	22.81%	99%	44%	42%	-
44	gp132	Uncharacterized protein	12	20422.20	20312.2	3	29.01%	99%	64%	66%	-
45	gp154	Structural head protein	12	21118.50	21008.5	8	67.80%	100%	52%	53%	-
46	gp155	Major head protein	2	83044.70	82934.7	27	72.03%	98%	67%	63%	98%
47	gp159	Uncharacterized protein	2	81323.90	81213.9	7	12.80%	98%	43%	34%	98%
48	gp161	Structural protein	14	16948.80	16838.8	4	43.45%	96%	-	35%	99%
49	gp162	Structural protein	9	33581.10	33471.1	10	38.19%	98%	40%	36%	99%
50	gp163	Structural head protein	2	84447.10	84337.1	19	38.23%	99%	57%	49%	99%
51	gp164	Structural protein	2	100450.10	100340.1	19	33.75%	97%	56%	55%	-
52	gp165	Structural protein	7	48629.30	48519.3	11	37.94%	99%	53%	54%	-

53	gp166	Tail tip protein	2	85 168.40	85058. 4	24	51.53 %	97 %	41%	38%	-
54	gp167	Structural protein	14	12 741.90	12631. 9	5	54.72 %	95 %	46%	45%	-
55	gp168	Structural protein	6	53 074.90	52964. 9	11	32.97 %	99 %	40%	38%	99 %
56	gp169	Structural protein	6	51 629.20	51519. 2	10	35.23 %	99 %	39%	35%	28 %
57	gp170	Structural protein	6	52 794.50	52684. 5	17	54.49 %	98 %	47%	38%	25 %
58	gp171	Uncharacterized protein	11	24 417.30	24307. 3	6	42%	100 %	36%	35%	-
59	gp173	Uncharacterized protein	13	20 064.30	19954. 3	3	22.22 %	99 %	46%	40%	-
60	gp174	Structural protein	8	33 824.80	33714. 8	12	73.65 %	99 %	70%	66%	-
61	gp176	Structural protein	12	19 664.70	19554. 7	2	12.80 %	98 %	30%	-	-
62	gp179	Structural protein	12	20 550.00	20440	7	43.43 %	98 %	45%	45%	99 %
63	gp180	Endolysin*	9	30 282.90	30172. 9	8	46.03 %	97 %	47%	44%	51 %
64	gp181	Putative tail sheath protein	2	85 190.00	85080	31	77.35 %	98 %	55%	41%	98 %
65	gp182	Putative tail fiber protein	1	116 150.10	11913 0	38	72.58 %	97 %	36%	28%	97 %
66	gp184	Uncharacterized protein	12	19 939.70	18480	4	30.36 %	98 %	25%	-	-
67	gp185	β/β′-like virion-associated protein	10	26 098.10	24640	11	63.84 %	99 %	67%	62%	-
68	gp188	Uncharacterized protein	6	55 385.50	52470	5	14.46 %	99 %	80%	70%	-
69	gp189	Structural head protein	8	34 215.70	33000	14	89%	99 %	32%	28%	-
70	gp194	Structural head protein	6	51 221.40	48510	25	86.17 %	99 %	58%	53%	-
71	gp195	Uncharacterized protein	8	36 016.30	34760	9	39.87 %	100 %	39%	38%	-
72	gp196	Uncharacterized protein	14	16 784.10	14740	3	52.24 %	99 %	26%	-	99 %
73	gp197	Structural protein	13	17 896.10	17270	6	65.60 %	99 %	-	-	-
74	gp198	Uncharacterized protein	10	24 279.80	22990	8	66.99 %	99 %	46%	42%	-
75	gp199	Structural head protein	5	58 593.30	56980	22	51.93 %	99 %	-	-	-
76	gp200	Structural head protein	7	44 512.30	43010	16	60.10 %	99 %	52%	44%	-
77	gp209	Uncharacterized protein	10	20 225.00	18590	3	22.48 %	99 %	45%	35%	-
78	gp214	Structural protein	7	41 360.80	38720	13	73.01 %	99 %	41%	38%	99 %
79	gp215	Head protease	9	31 928.10	29700	12	64.07 %	100 %	60%	56%	-
80	gp216	Structural head protein	10	27 850.00	26400	9	60.42 %	100 %	70%	63%	10 0%
81	gp217	Structural head protein	5	61 170.50	56210	19	72.99 %	98 %	48%	41%	-

82	gp219	β/β′-like virion-associated protein	1	167 516.50	158510	51	51.56 %	99 %	58%	53%	-
83	gp220	β/β′-like virion-associated protein	3	63 084.20	59840	18	49.63 %	97 %	75%	68%	98 %
84	gp221	Structural peptidoglycan hydrolase	1	246 430.90	242330	62	37.90 %	98 %	37%	34%	98 %
85	gp222	Structural protein	3	77 193.00	71720	17	37.42 %	97 %	64%	63%	98 %
86	gp228	Uncharacterized protein	14	13 039.60	11990	2	24.22 %	100 %	-	-	-
87	gp229	Thymidylate kinase*	7	40 994.40	38720	12	49.15 %	100 %	35%	32%	-
88	gp232	Uncharacterized protein	10	30 790.70	28710	3	18.77 %	97 %	-	-	95 %
89	gp239	Uncharacterized protein	13	19 305.20	17600	3	23.75 %	98 %	46%	41%	-
90	gp240	Structural protein	14	17 449.40	15730	2	19.58 %	100 %	60%	62%	-
91	gp241	Uncharacterized protein	10	25 888.40	24090	6	38.36 %	99 %	43%	36%	98 %
92	gp242	Structural protein	3	72 744.80	70950	13	28.68 %	99 %	34%	28%	98 %
93	gp243	Structural protein	13	18 071.50	17160	4	57.05 %	100 %	-	-	99 %
94	gp244	Structural protein	2	83 120.40	76670	23	37.45 %	99 %	58%	51%	99 %
95	gp248	Uncharacterized protein	10	29 676.40	25960	2	10.17 %	100 %	-	24%	-
96	gp262	Uncharacterized protein	14	10 000.80	7590	2	24.64 %	97 %	-	-	97 %
97	gp269	Structural protein	14	17 955.30	15070	4	35.04 %	100 %	41%	33%	99 %
98	gp273	Structural protein	8.9	23 729.20	21890	4	20.60 %	100 %	-	-	-
99	gp279	Uncharacterized protein	8	35 239.80	33220	2	14.24 %	100 %	-	-	-
100	gp284	Thymidylate synthase*	5	58 214.90	53680	2	5.94 %	99 %	46%	60%	-
101	gp296	Structural protein	14	15 184.00	12980	4	50.85 %	99 %	32%	-	98 %
102	gp298	Uncharacterized protein	11	25 232.70	23100	2	15.24 %	96 %	-	-	-
103	gp339	Uncharacterized protein	12	20 495.30	18810	3	19.30 %	100 %	57%	57%	-
104	gp342	Uncharacterized protein	8	34 070.20	31900	5	19.65 %	93 %	-	-	97 %
105	gp346	Uncharacterized protein	12	26 364.50	23870	2	11.06 %	98 %	48%	40%	99 %
106	gp352	Uncharacterized protein	14	17 830.30	14190	8	66.67 %	88 %	-	-	97 %
107	gp354	Uncharacterized protein	14	7 495.30	6380	2	32.76 %	91 %	-	-	95 %
108	gp358	Uncharacterized protein	12	21 849.80	19140	2	16.09 %	63 %	60%	30%	63 %
109	gp359	Structural protein	8	37 136.40	36630	8	47.75 %	97 %	53%	-	96 %
110	gp365	Structural protein	3	72 814.60	68090	19	45.23 %	76 %	-	-	98 %

111	gp367	Ribonucleoside reductase*	7	45 827.80	41910	9	28.08 %	98 %	75%	64%	-

*enzymes non-associated with phage particles

906 **Table S2.** Phage activity comparison of fourteen different *Pseudomonas* phages on *P. aeruginosa* strains from
907 Military Hospital Nederoverheembeek, Brussels, Belgium collection [Pirnay JP et al., 2002].

	***PA* strains**	**KTN4**	**KTN6**	**KT28**	**KMV**	**LKD16**	**LUZ19**	**LKA1**	**LIT1**	**LUZ7**	**LUZ24**	**LSL4**	**LMA2**	**LBL3**
1	US449	■					■			■			■	
2	LMG14083	■	■	■										
3	Bu007	■	■	■								■		■
4	PAO23		■	■		■	■			■	■			■
5	Aa 249													
6	US448	■	■	■			■		■		■	■	■	■
7	PAO1 Krylov	■	■	■	■	■	■	■		■	■			■
8	Lo050									■	■			■
9	US450		■	■	■	■	■			■	■			■
10	Li004	■	■		■	■	■		■					
11	Be128		■	■	■					■	■	■		
12	Lo053		■	■										
13	ATCC 27853	■	■	■	■	■	■		■	■				■
14	Br906	■	■	■	■				■	■		■	■	■
15	PhDW6	■	■	■	■	■	■		■	■			■	■
16	So099		■	■							■			
17	Aa 245		■	■	■								■	
18	LMG5031									■				■
19	C17	■	■		■	■	■							
20	C19			■						■				
21	Lo049													
22	Br642	■	■	■								■	■	■
23	Li012			■								■		
24	Is579		■	■										
25	C	■	■	■						■				
27	Lw1047								■					
28	Br257	■	■		■	■	■		■	■	■			■
29	Br667													
30	C18	■	■		■	■	■							
31	LMG2107	■	■	■	■	■	■			■	■	■	■	■
32	Bu004													
33	C1	■	■	■			■			■				
34	PAO29													
35	C13		■	■							■			■
36	C2	■												■
37	Aa 246		■	■	■	■	■			■			■	■
38	LMG14084	■	■	■										
39	Br735			■										
40	Mi162		■	■						■				■
41	SG17M	■	■		■	■	■				■			■
42	Pr335	■	■	■	■	■	■						■	■
43	Is580	■	■	■								■	■	■
44	Li009	■	■							■			■	
45	Be136	■	■	■	■	■	■	■		■		■	■	■
46	Is573		■											■
47	Br908		■										■	
48	TuD199		■	■	■	■	■			■				■
49	So095			■										
50	So092			■								■		■
51	Br229					■	■							
52	SG50M	■	■	■										■
53	PT31M	■	■		■	■	■				■			■

54	Mi151													
55	US447													
56	Bo548													
57	Br680													
58	PA6													
	Summary	27	39	34	19	18	23	2	7	20	13	10	14	27
	% of the tested strains	46.6	67.2	58.6	32.7	31.0	39.7	3.5	12.1	34.5	22.4	17.2	24.1	46.6

908 grey box –active, white box – no activity.
909
910

911 **Table S3.** The Nephrophane roughness (R) parameters measured by ZET 20.

Markers	Probe [mean ± SD]		
	Nephrophane	**Nephrophane covered by PAO1 biofilm**	**Nephrophane covered by PAO1 biofilm treated with KTN4 phage**
Ra	2.364 ± 0.2205	2.348 ± 0.3176	2.373 ± 0.3124
Rq	2.927 ± 0.3044	2.898 ± 0.3526	2.990 ± 0.4030
Rpv	16.11 ± 2.057	14.52 ± 2.301	16.38 ± 2.435
Rp	8.591 ± 1.312	8.156 ± 1.337	8.496 ± 1.762
Rv	7.515 ± 1.203	6.365 ± 1.242	7.880 ± 1.326
Rsk	0.0830 ± 0.2326	0.3990 ± 0.2897*	0.1445 ± 0.3906

912

913

Supplementary Results

Genome and proteome analysis of KTN4

Using high throughput sequencing by the Illumina MiSeq platform, the complete genome sequence was determined. KTN4 has a linear, circularly permutated and terminally redundant, A+T-rich (36,9% GC) double-stranded DNA molecule (279,593 bp). In total, 368 open reading frames (ORFs) could be predicted, varying in size from 36 to 2237 amino acid residues, as well as six tRNAs (Leu (UUA), Pro (UUG), Met (CAU), Asp (GUC), Asn (GUU), Thr (UGU) . Of these, 87 proteins have a predicted function. According to the orientation of transcription, ORFs are organized into operons and most are on a positive strand. The KTN4 shows a genome-wide nucleotide sequence similarity to: phiKZ 99%, PA7 99%, phiPA3 84%, 201phi2-1 78% (BLAST). As such, it can be defined as an isolate of the *Pseudomonas* phage phiKZ species. However, there are few significant differences. Genome of KTN4 lacks phiKZ gp24.1 (frame shift caused by two deletions) and gp24.2 (point mutation). In this position, there is a clear sequence of gp34 KTN4 on a positive strand. Also phiKZ gp70.1 is absent, showing only 58,27% nucleotide sequence similarity to the KTN4 genome. Two genes (KTN4 gp93 and gp94) show less than 60% nucleotide similarity to phiKZ genome and several genes have no similarity (KTN4 gp23-26, gp30-32, gp75, gp286-287, gp325, gp321). Finally, two additional proteins were annotated, which are also present in phiKZ genome and corrected according phiKZ RNA-seq (KTN4 gp14, 97.70% homology and gp59, 98,60% homology). None of these genes have a predicted function. Based on phiKZ RNA-seq analysis performed previously by Ceyssens P.J *et al.* (Ceyssens et al. 2014) and using the PISE EMBOSS fuzznuc program, 47 promoters were predicted for phage KTN4. Among them, 31 are early phage-specific promoters with highly conserved, uni-directionally distributed AT-rich intergenic motifs (5'-TATATTAC-3') (Fig. S2 A). Furthermore, less conservative upstream (5'-TTTaA-3') and downstream (5'-TG-3') motifs were found. The middle promoters are located on both strands

and distributed throughout the whole genome. They are linked by only a weak AT-rich motif (5'-AAanntTAC-3'; lowercase letters represent a lower level of conservation) centered at position 24 with respect to the transcription start site (Fig. S2 B). For late transcription no sequence conservation upstream of 5' ends could be detected apart from a 5'-TATG-3' motif overlapping the transcription start site (11 late promoters) (Fig. S2 C). Using ARNOLD software, 107 of putative factor-independent terminators were predicted. Most potential stem-loop transcription terminators contain the tetranucleotide UUCG loops (Fig. S3). Using ESI-MS/MS analysis of proteins from denaturated phage particles fractionated on SDS-PAGE, 111 gene products have been identified, among which five virion-unrelated enzymes, 36 virion-associated proteins and 70 structural gene products, with sequence coverages ranging between 5,94% to 89% (Fig S4, Table S1). The KTN4 structural proteins were compared to their homologues from phiKZ (NC_004629.1 from 2008 and AF399011.1 from 2013), PA7 (JX233784.1), PhiPAK3 (HQ630627.1) and 201phi2-1 (NC_010821.1) phages (BLASTP). As expected, the highest similarity was found for phiKZ structural proteins, ranging from 63% to 100%, except for gp93, which was identical to PA7 hypothetical protein (AFO71119.1). Twenty two structural head proteins were identified including gp215 head protease identical to phiKZ gp175 and a major head protein gp155 with 98% similarity to phiKZ gp120 (Thomas et al. 2012), The contractile tail of phiKZ, the closes homologue to KTN4, is built from at least 32 different proteins, but a definitive structural function was assigned to only two of them: the tail sheath protein (KTN4gp39 versus phiKZ gp29) and the tail tip protein (KTN4 gp166 versus phiKZ gp131). Tail tip protein is located at the periphery of the baseplate and possibly associates with fibers that emanate from the baseplate. In the ESI-MS/MS analysis two additional proteins were identified gp181 (putative tail sheath protein) and gp182 (putative tail fiber). The presence of tail associated enzyme gp221 (structural peptidoglycan hydrolase) corresponded to gp181 of phiKZ phage. This enzyme cleaves the host cell wall during the first

964 stage of the life cycle (Briers et al. 2008). In the centre of the phiKZ baseplate, there is a density
965 that resembles the needlelike ‘‘cell-puncturing’’ device of T4, which is most likely composed
966 of gp181. Further analysis reveal gp52, that represents a chain A of monomeric subunit of Tubz,
967 protein believed to be essential for the correct centering of replicated bacteriophage virions
968 within the bacterial host. Moreover, four β/β′-like virion-associated proteins in KNT4 phage
969 (gp106, gp185, gp219, and gp220) were assigned as a non-canonical multi-subunit viral RNA
970 polymerase (RNAP) similar to phiKZ gp80, gp149, gp178, gp180 (Ceyssens et al. 2014).
971 During ESI-MS/MS analysis we were not able to identify any peptide corresponding to gp202
972 (phiKZ gp164) and gp224 (phiKZ gp 184) (Ceyssens et al. 2014). Furthermore, the analysis of
973 phiKZ RNAP performed by (Yakunina et al. 2015) allowed to identify five homologous
974 subunits in KTN4 genome, the products of early phage genes. Four of these are cellular RNAP
975 subunits homologs of the non-virion set (nvRNAP): 1) gp74, homologous to gp55 phiKZ,
976 however shorter by 41 amino acids; 2) gp95 and gp96 (phiKZ gp71 and gp73); phiKZ gp72, a
977 part of phiKZ subunit has no homologue in KTN4 genome; 3) gp97 identical to gp74 phiKZ
978 and 4) gp158 identical to gp123 phiKZ. The fifth subunit, gp90 identical to gp68 phiKZ, is a
979 protein of unknown function with no similarity to known RNAP subunits or any other known
980 protein family. Gp74 and gp97 together correspond to msRNAP largest (bacterial β’) subunits
981 and gp95 and gp96 subunit corresponds to the C-terminal half of msRNAP second largest (β in
982 bacteria) subunits. Gp158 is highly diverged homolog of the N-terminal half of the second
983 largest (β in bacteria) msRNAP subunits. This complex initiates transcription from late
984 promoters in rifampicin-resistant manner, tested *in vitro* in phiKZ, which suggests that virus
985 relies on its own transcription machinery for the entire infection process. However, the late
986 promoter 5’-TATG-3’ conserved motif is necessary for transcription by nvRNAP *in vitro*
987 (Yakunina et al. 2015). The endolysin of KTN4 (gp180) is highly identical (99%) to the
988 endolysin of *P. aeruginosa* phiKZ gp144. This endolysin is well studied both at the molecular,

biochemical (Briers et al. 2007; Briers et al. 2008; Cloutier et al. 2010) and structural level (Fokine et al. 2008). The consensus motifs for peptidoglycan binding (underlined) and the catalytic residue (boxed) are fully conserved in KTN4 gp180.

The protein sharing network for jumbo phage KTN4 is presented in Fig. 1. A resulting network comprises 495 phages (nodes) belonging to *Myoviridae*, *Siphoviridae*, *Podoviridae*, or uncharacterized and other phages and 6,948 relationships (edges) between them (Fig. 1A). In this graph, phage KTN4 was placed in a single component with five well-known *Pseudomonas* phiKZ-related phages including phiKZ, phiPA3, 201phi2-1, EL and OBP (Cornelissen et al. 2012), as well as phages phiJM-2012, SPN3US, CR5, and phiEaH2, which was separated from other components. When the network topology was computed with two classical measures such as the clustering coefficient (CL) and betweenness centrality (BC) (Brohée et al. 2008), this component shows the highest CL =1 (absolute cohesiveness) and the lowest BC = 0 (none of node acting as a bridge among other pairs of nodes). This network structure reflects the distinct core gene-sets shared between their genomes (Jang et al. 2013b), which form a tight-knit clique of full interconnectivity. Next, the connectivity pattern of this component has been investigated not only on the basis of protein sequence identities, but also according to phage-phage similarity score after normalizing the number of shared genes between genomes (Leplae et al. 2010) (Lima-Mendez et al. 2008). As a result, over the threshold of 60% identity, phages KTN4, phiKZ, phiPA3, and 201phi2-1 kept forming an in-group relationship with phiKZ being the closest relative to KTN4 (Fig. 1B). In addition, KTN4 was more closely related to phiKZ, phiPA3, and 201phi2-1 with the phage-phage similarity score ranging from 157.2 to 999.9, indicating more shared homologous genes between them than others. The other *Pseudomonas* phages including EL and OBP were connected for identity values less than 35% and similarity score, 79.9. The phages phiEaH2, SPN3US, CR5, and phiJM-2012, having different host ranges

(i.e., *Erwinia*, *Salmonella*, *Cronobacter*, and *Vibrio* sp., respectively), were weakly connected to other phiKZ-related members in terms of both shared gene contents and sequence identity. The genetic relationships of KTN4 have been investigated by constructing a mathematical model of gene (protein)-sharing network, extending to possible close relatives. In our phage population network, KTN4 is constricted to a single isolated component comprising the five *Pseudomonas* phiKZ-related phages and other potential relatives. Subsequent network decomposition strongly indicates that KTN4 belongs to the "phiKZ-like viruses", subdivision of the phiKZ-related groups (Cornelissen et al. 2012), with the large proportion of phiKZ-specific core gene-sets in common to the phiKZ, phiPA3, and 201phi2-1. More specifically, the connectivity patterns suggest that phiKZ appears to be the closest relative to KTN4 as their protein families with more than 90% sequence identity can be considered more recently shared than those of other phage members in this group (Halary et al. 2010). In addition, our population network can reveal other informative connections. The phages phiEaH2, SPN3US, and CR5 were found to interconnect solely with the phiKZ-related phages, indicating that they are probably diverged member of the phiKZ-related group as observed in phiJM-2012 (Jang et al. 2013b). These results suggest that the phiKZ-like phages' diversity has not been fully delimited and that there are additional more distant relatives yet to be discovered.